The DELPHI silicon tracker at LEP2

P. Chochula, P. Rosinsky, A. Andreazza, G. Barker, V. Chabaud, P. Collins,
H. Dijkstra, Y. Dufour, M. Elsing, P. Jalocha, et al.

The DELPHI Silicon Tracker at LEP2

The DELPHI Silicon Tracker Group

P. Chochula, P. Rosinský

Comenius University Bratislava, Faculty of Mathematics and Physics, Mlynskà dolina,
SK-84215 Bratislava

A. Andreazza, G. Barker, V. Chabaud, P. Collins, H. Dijkstra, Y. Dufour*, M. Elsing,
P. Jałocha, Ch. Mariotti, K. Mönig, D. Treille, A. Zalewska.
CERN, CH-1211, Geneva23, Switzerland

F. Ledroit

ISN Grenoble, Institut des Sciences Nucléaires, 53 Avenue des Martyrs, F-38026 Grenoble
Cedex, France

C. Eklund, R. Orava, K. Österberg, H. Saarikko, R. Vuopionperä

Helsinki Institute of Physics, HIP and Department of Physics, University of Helsinki, P.O.
Box 9, FIN-00014 Helsinki, Finland

W. de Boer, F. Hartmann, S. Heising, M. Kaiser, D. Knoblauch, G. Maehlum, M. Wielers

Inst. für Exper. Kernphysik - Universität Karlsruhe, Engesserstrasse 7, D-76128 Karlsruhe,
Germany

P. Brückman, K. Gałuszka, T. Gdański,W. Kucewicz, J.Michałowski, H.Pałka.

High Energy Physics Laboratory, Institute of Nuclear Physics, ul. Kawiory 26a,
PL-30055 Kraków, Poland

V. Cindro, E. Križnič, D. Žontar

Univerza v Ljubljani, Institut Jozef Stefan, Jamova 39, P.O.B. 3000, SI-1001 Ljubljana,
Slovenija

J.C. Clemens, M. Cohen-Solal, P. Delpierre, T. Mouthuy, M. Raymond, D.Sauvage

CPPM Faculté des Sciences de Luminy, Université Aix Marseille II, 70 Route Léon Lachamp,
F-13288 Marseille, France

E. Bravin, M. Caccia, R. Campagnolo, F. Chignoli, R. Leoni, C. Meroni, M. Pindo,
C. Troncon, G. Vegni

Dipartimento di Fisica, Università di Milano and INFN, Via Celoria 16, I-20133 Milano, Italy

F. Couchot, B. D'Almagne, F. Fulda, A. Trombini

Université de Paris-Sud, Lab. de l'Accelérateur Linéaire, IN2P3-CNRS, Bât. 200,
F-91405 Orsay Cedex, France

J. Bibby, N. Demaria, P. Pattison, N. Vassilopoulos

Dept. of Nuclear Physics, Univ. of Oxford, Keble Road, Oxford OX1 3RH, UK

M. Mazzucato, A. Nomerotski, I. Stavitski

Dipartimento di Fisica, Università di Padova and INFN, Via Marzolo 8, I-35131 Padova, Italy

J.M. Brunet, B. Courty, G. Guglielmi, J.J. Jaeger, G. Tristram, J.P. Turlot
*Collège de France, Lab. de Physique Corpusculaire, IN2P3-CNRS, F-75231 Paris Cedex 05,
France*

M. Baubillier, L. Roos, F. Rossel
*LPNHE, IN2P3-CNRS, Universités Paris VI et VII, Tour 33 (RdC), 4 place Jussieu,
F-75252 Paris Cedex 05, France*

R. Leitner, J. Masik, J. Ridky, P. Sicho, V. Vrba.
*Institute of Physics, Academy of Sciences and Nuclear Center, Faculty of Mathematics and
Physics, Charles University, Praha 8, Czech Republic*

M. Bates, J .Bizzell, L. Denton, P. Phillips
Rutherford Appleton Lab., Chilton, Didcot OX11 OQX, UK

M. Gandelman, E. Polycarpo
*Univ. Federal do Rio de Janeiro, C.P. 68528 Cidade Univ, Ilha do Fundão, BR-21945-970
Rio de Janeiro, Brazil*

C. Bosio, V. Rykalin
*INFN, Istituto Superiore di Sanità, Sezione Sanità, Viale Regina Elena 229, I-00161 Roma,
Italy*

C. Martinez-Rivero
*Universidad de Cantabria, Facultad de Ciencias, C/Avda. Los Castros, S/N, E-39005
Santander, Spain*

R. Brenner, O. Bystrom
*ISV- Department of Radiation Sciences, University of Uppsala, P.O. Box 535, S-751 21
Uppsala, Sweden*

W. Adam, N. Frischauf, M. Krammer, G. Leder, H. Pernegger, M. Pernicka, D. Rakoczy
*Institut für Hochenenergiephysik, Oesterreichische Akademie der Wissenschaften,
Nikolsdorfergasse 18, A-1050 Wien, Austria*

K.H. Becks, J. Drees, P. Gerlach, K.W. Glitza, J.M. Heuser, S. Kersten, B. Überschär
*Gesamthochschule Wuppertal Bergische Universität, Fachbereich Physik, Postfach 100127,
Gausstrasse 20, D-42097 Wuppertal, Germany*

* Yves was one of the driving forces during the design and construction of the Silicon Tracker. He was killed in an avalanche on the Pointe Percée in January 1996, a victim of his passion for the high mountains. We would like to dedicate this paper to his memory.

Abstract

The DELPHI Silicon Tracker, an ensemble of microstrips, ministrips and pixels, was completed in 1997 and has accumulated over 70 pb^{-1} of high energy data. The Tracker is optimised for the LEP2 physics programme. It consists of a silicon microstrip barrel and endcaps with layers of silicon pixel and ministrip detectors. In the barrel part, three dimensional b tagging information is available down to a polar angle of 25°. Impact parameter resolutions have been measured of 28 μm $\oplus$ 71/($p \sin^{\frac{3}{2}} \theta$) μm in $R\phi$ and 34 μm $\oplus$ 69/p μm in Rz, where p is the track momentum in GeV/c. The amount of material has been kept low with the use of double-sided detectors, double-metal readout, and light mechanics. The pixels have dimensions of 330 × 330 μm^2 and the ministrips have a readout pitch of 200 μm. The forward part of the detector shows average efficiencies of more than 96%, has signal-to-noise ratios of up to 40 in the ministrips, and noise levels at the level of less than one part per million in the pixels. Measurements of space points with low backgrounds are provided, leading to a vastly improved tracking efficiency for the region with polar angle less than 25°.

3

1   Introduction

The DELPHI Silicon Tracker presented in this paper has been optimised to cope with the requirements posed by the physics programme at LEP2. The design [1] had to take into account the following features of the processes studied or searched for:

- Four fermion processes, important for both standard and non-standard physics, are relatively frequent, hence a larger angular coverage in polar angle[1] is required compared to Z° physics.

- In the processes with the largest cross sections, such as $e^+e^- \to q\bar{q}\gamma$ or $e^+e^- \to \gamma\gamma$, the particles are produced predominantly in the forward direction.

- The search for the Higgs boson and for supersymmetric particles are important physics objectives for LEP2, so a good tagging of b quarks down to low polar angles is important in order to reduce background from standard processes such as W^+W^- production.

2   Design Considerations

The Silicon Tracker uses different kinds of technologies in each angular region in order to achieve the performance goals discussed above. Two main tasks can be distinguished:

- Vertexing in the barrel region

  The central part of the Silicon Tracker must have a b-tagging performance which is at least equivalent to that of the 1994-95 Vertex Detector [2], and in addition be extended down to around 25°, beyond which multiple scattering starts to dominate the impact parameter resolution for b hadron decay products. This is achieved with three layers of microstrip modules, termed Closer, Inner and Outer, at average radii of 6.6 cm, 9.2 cm and 10.6 cm. In the $R\phi$ plane the resolution is around 8 μm, and in the Rz plane the readout pitch is changed for plaquettes at different angles to give the best resolution possible perpendicular to the track, varying between about 10 μm and 25 μm for tracks of different inclination. The material is kept to a minimum by the use of double-sided detectors and light mechanics. This part is called the Barrel.

- Tracking in the forward region

  In the forward region, the emphasis is on improved momentum measurement and standalone pattern recognition. The detector must improve the overall hermeticity of DELPHI and provide a better extrapolation of tracks towards the forward RICH [3] detectors, leading to a better particle identification in this region. The momentum measurement is limited by Coulomb scattering and a resolution of about 100 μm is sufficient. These requirements are met [1] by adding silicon endcaps, consisting of two layers of pixel detectors, with pixel dimensions of 330×330 μm², and

---

[1]In the standard DELPHI coordinate system, the z axis is along the electron direction, the x axis points towards the center of LEP, and the y axis points upwards. The polar angle to the z axis is called θ and the azimuthal angle around the z axis is called ϕ; the radial coordinate is $R = \sqrt{x^2 + y^2}$.

two layers of back-to-back ministrip detectors with a readout pitch of 200 μm and one intermediate strip. The pixel detectors have a noise level of less than one part per million which is crucial to eliminate ghost tracks, and the ministrips operate at a signal over noise of more than 40. To help the pattern recognition the ministrips are mounted at a small stereo angle. The angular accuracy is about 1 mrad, and the extrapolation accuracy at the forward tracking chambers of DELPHI is a few mm. This part is called the Very Forward Tracker (VFT).

Throughout the detector there is great emphasis on the overlap of sensitive silicon, within each layer of detectors, and between the different layers. This provides redundancy and allows a self alignment procedure, but places great constraints on the assembly, since silicon plaquettes from different layers are often separated by less than 1 mm.

To make the project affordable components and systems were re-used from the previous silicon vertex detectors of DELPHI, namely some of the plaquettes and hybrids [2] and the data acquisition and service systems [4]. The complete Barrel and a large part of the VFT (the full set of ministrip detectors and 60% of the pixels) was in operation during the 1996 data taking. The complete detector was installed in DELPHI for the data taking in 1997.

The Silicon Tracker is illustrated in figure 1. The three concentric layers of the barrel detector cover the angular region $21° - 159°$. Two pixel layers, the first one being located inside the barrel, and two ministrip detector endcaps cover the angular region $11° - 26°$ and $154° - 169°$. As an illustration of its physics capabilities we show in figure 2 an event registered in 1996 at the energy $\sqrt{s} = 161$ GeV, where a jet with $\theta = 35°$ is tagged as a b jet.

Full technical descriptions of the detector and the individual layers can be found in [5]- [9]. In what follows we give a summary only, mentioning in particular the new features.

3   Silicon Components

The characteristics of the silicon plaquettes used are summarised in table 1 and figure 3. The suppliers used were Hamamatsu[2], SINTEF[3], CSEM[4] and MICRON[5].

Multiple scattering at the first measured point dominates the track impact parameter resolution. In order to minimise the amount of material the Closer layer is composed of double-sided detectors. This layer is taken from the 1994-95 Vertex Detector [2]. For the Outer layer, where multiple scattering is less crucial, a cheaper back-to-back solution was chosen. This layer is completely new, and has a novel Rz measurement which is made with single-sided detectors with p^+ implants, with the signals being routed to the ends of the detectors with a double-metal technique. The diodes are either read out singly, or singly with one intermediate strip, or ganged in pairs, with two connected intermediate strips. This gives a choice of pitches, allowing the resolution to be optimised for tracks passing through at different incidence angles. The Inner layer is built up of both double and single-sided detectors, allowing the re-use of double-sided detectors from the previous vertex detector.

---

[2]Hamamatsu Photonics K.K., Hamamatsu City, Japan
[3]SINTEF, Oslo, Norway
[4]CSEM,Rue de la Maladiére 41, CH 2007, Neuchatel, Switzerland
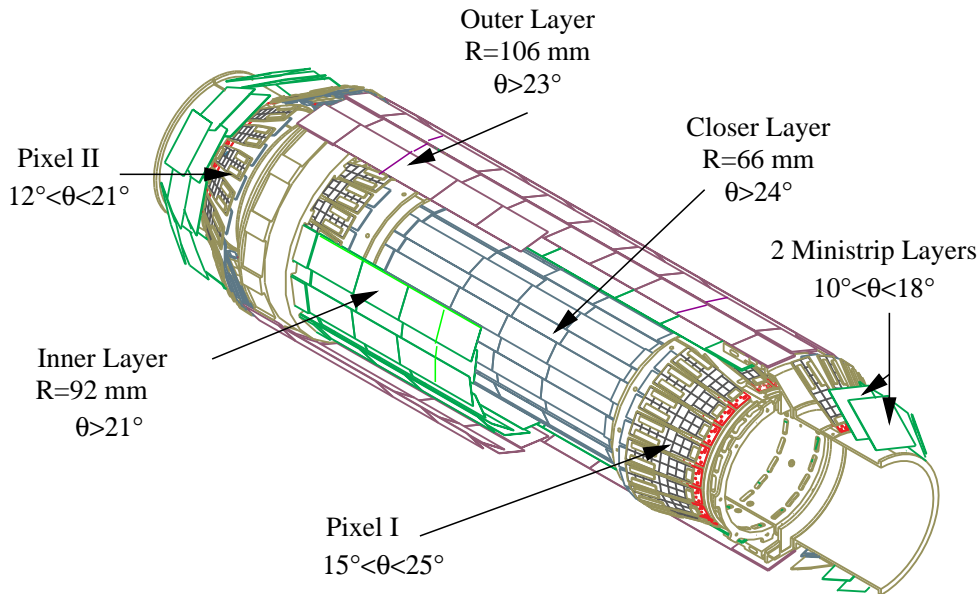[5]MICRON Semiconductor Limited, Sussex BN15 8UN, England

Figure 1: Layout of the DELPHI Silicon Tracker

The pixel plaquettes are divided into ten regions of 24×24 pixels at large radius and six regions of 24×16 pixels at smaller radius. Each region is read out by an SP8 [10] chip bump-bonded to the detector (see section 4). The pixel size is 330×330 μm^2, and pixels at the boundary between neighbouring read-out chips have increased dimensions, so that blind regions in the active area are avoided. The ministrip plaquettes have a readout pitch of 200 μm with one intermediate strip.

4   Assembly into Modules and Crowns

The concept of the Silicon Tracker is modular: the plaquettes in each region are assembled into electrically independent modules or crowns, which are subsequently connected to their repeater electronics and mounted onto the support structure. The characteristics of these modules and crowns are summarised in table 2.

In the barrel the modules take the form of ladders 4 or 8 plaquettes in length, each of which forms an electrically independent half of a barrel module. The front-end electronics are mounted onto double-sided BeO hybrids at each end of the modules, and multilayer kapton cables join the hybrids to the repeaters. In each quarter of the detector there is one repeater card per layer, serving 10 or 12 modules. Bond wires connect the signal and bias lines between the detectors and hybrids. In the Inner layer this leads to one bias line connecting together diodes with polysilicon resistor and FOXFET biasing, which has been operating successfully. For the Closer and Inner layers the front end amplifier used is the MX6 [12], taken from the previous detector, and for the Outer layer the new
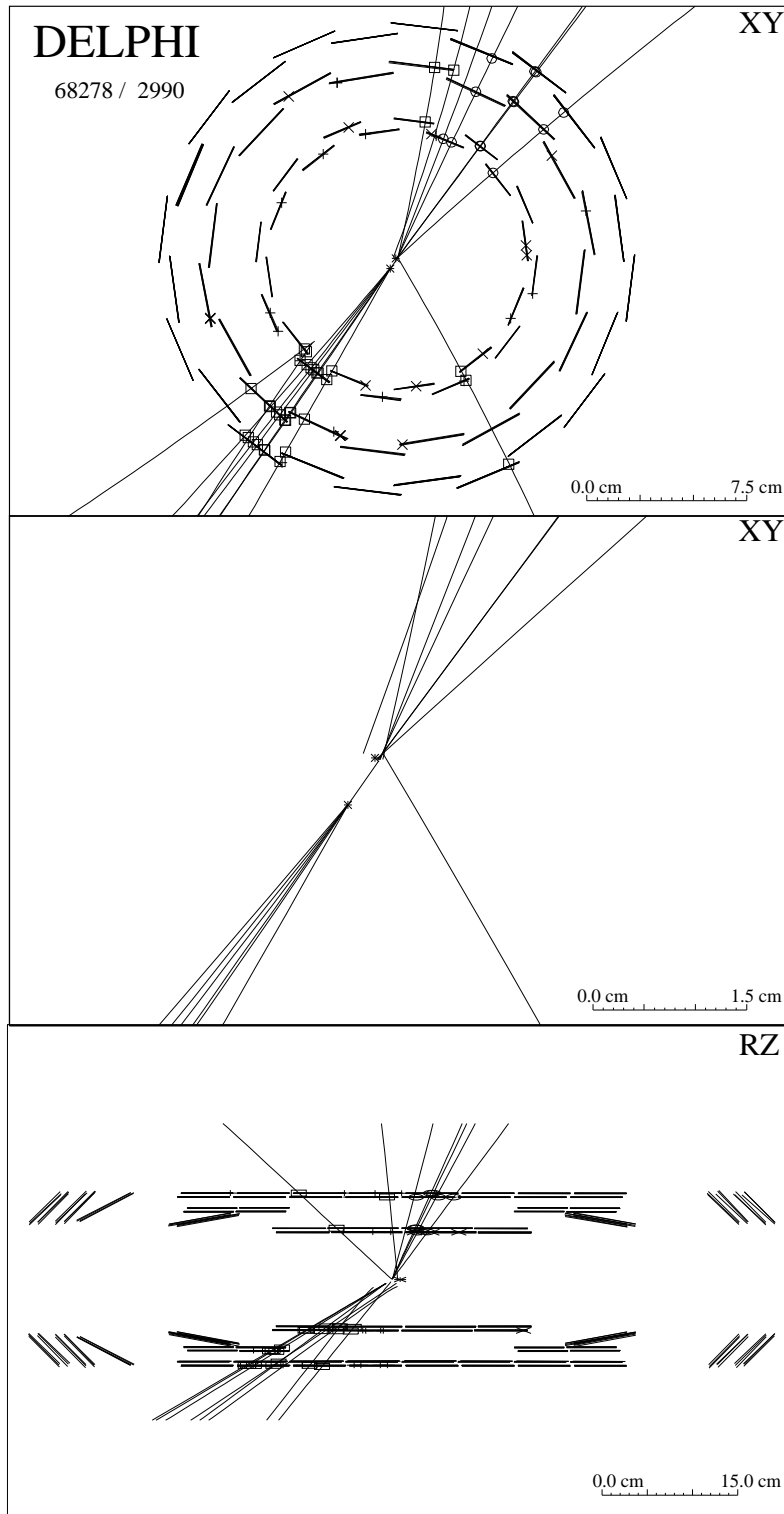
Figure 2: Event registered during the 1996 161 GeV run. The top two views show the $R\phi$ projection on two different scales. The displaced vertex is clearly seen. The bottom view displays the Rz projection. In 1996 only one quarter of the second pixel layer was installed.

Characteristics of silicon plaquettes	Barrel				VFT	
	a	**b**	**c**	**d**	Pixels	Ministrips
supplier	Hamamatsu	SINTEF	Hamamatsu	SINTEF	CSEM	MICRON
single/double-sided	ss	ss	ds	ds	ss	ss
double-metal p-side	no	yes	no	no	-	no
n-side	-	-	yes	yes	-	-
length (cm)	5.99	5.99	5.75	6.07,7.91	6.9	5.3
width (cm)	3.35	3.35	3.35	2.08	$1.7 - 2.2$	5.3
sensitive area (cm^2)	18.6	17.9	34.2	22.2,29.4	9.9	27.0
pitch (μm) p-side	25	44	25	25	330×330	100
n-side	-	-	42	49.5,99,150	-	-
readout pitch p-side	50	44,88,176	50	50	330×330	200
(μm) n-side	-	-	42,84	49.5,99,150	-	-
blocking strip (n-side)	-	-	p^+	field plate	-	-
# readout channels	640	640	640×2	384×2	8064	256
wafer thickness (μm)	290	310	320	310	$290 - 320$	300
implant width (μm)	8	8	12,14	6,8	-	60
biasing	FOXFET	Polysilicon resistors	Polysilicon resistors	Polysilicon resistors	DC	FOXFET
readout coupling	AC	AC	AC	AC	DC	AC
resistivity ($k\Omega$cm)	$3 - 6$	$3 - 6$	$3 - 6$	$3 - 6$	10	10
operating voltage (V)	60	60	65	$60 - 95$	$40 - 60$	60

Table 1: Characteristics of silicon plaquettes. There are 888 plaquettes in the full detector. The different types of plaquettes in the barrel, **a**, **b**, **c** and **d**, are arranged as shown in figure 3. Sensitive area counts $R\phi$ and Rz sides for cases of double-sided detectors.

DELPHI

OUTER LAYER
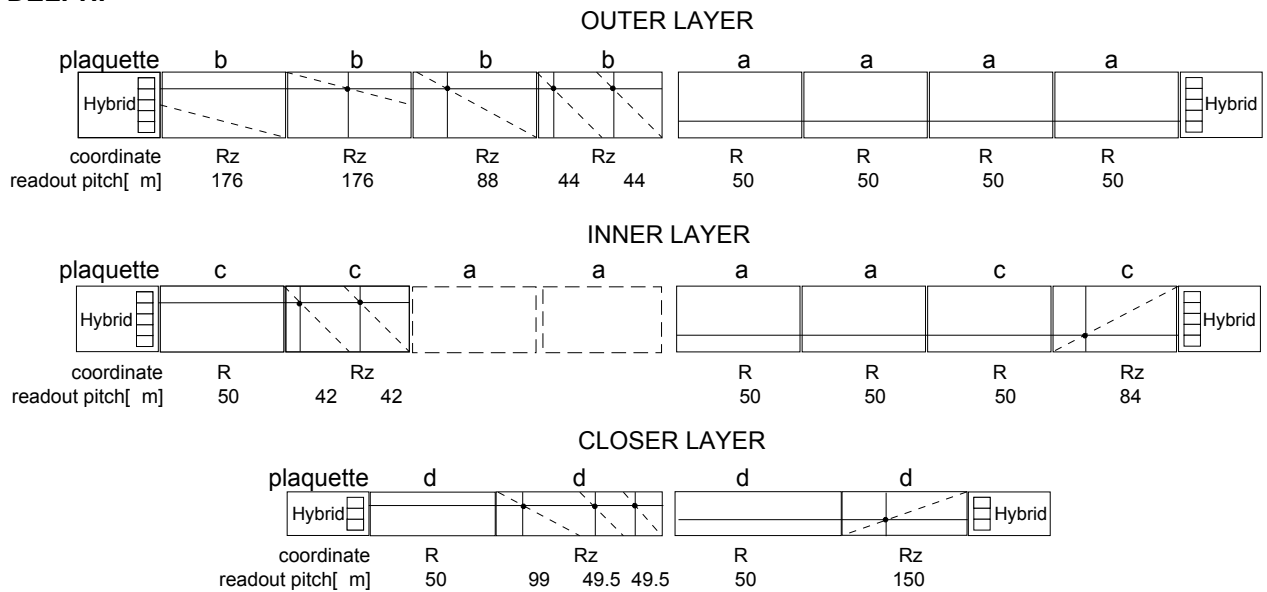

INNER LAYER

CLOSER LAYER

Figure 3: Arrangement of the detectors **a**, **b**, **c** and **d**, as defined in table 1, in the barrel. The left hand side of the figure illustrates the sides of the modules which face away from the beampipe, and the right hand side of the figure shows the sides of the modules which face towards the beampipe. The solid lines indicate the directions of the strips, and the dotted lines the layout of the contact holes in the case of double metal read-out. A full technical description of the components of the barrel and the readout conventions can be found in [11] .

TRIPLEX [13, 14] chip, with an Equivalent Noise Charge ENC = $(283 + 17 \times C_{\text{load}})$ electrons, where C_{load} is the load capacitance in pF. On the Rz side of this layer there is a charge loss in some plaquettes (up to a maximum of 25% in the most external plaquettes) due to the combination of the double-metal readout with intermediate strips [9], but due to the high S/N performance this leads to a negligible loss in resolution. The use of double-sided and back-to-back modules led to the choice of kevlar for the strengthening beams, with the addition of carbon fibre at the top of the beams to reduce the mechanical sensitivity to changes of humidity [15].

In the VFT, the pixel and ministrip plaquettes are mounted onto semicircular aluminium supports, with inclinations with respect to the z axis of 12° and 32° for the pixel and 49° for the ministrip plaquettes. The electronics are connected to the repeaters with kapton cables, with one repeater per crown for the ministrips and two repeaters per crown for the pixels.

The pixel plaquettes, each with 16 bump-bonded SP8 chips [10], are arranged in groups of 19 onto each pixel crown. Bus lines bringing the data and control signals to each of the chips are integrated onto the detector substrate using a double-metal process. This design reduces the amount of material and allows at the same time a reduction in the amount of signals by multiplexing on the integrated bus. On the other hand, it is a highly demanding design in terms of failure rate of the interconnection technique. The connection between the bus lines and the corresponding pad on the chip is achieved by the same bump-bonding technique used for the pixel interconnection. The IBM C4 (Controlled Collapse Chip Connection) bump bonding process [16] was used, and a $(2.4 \pm 0.2) \times 10^{-4}$ failure rate was achieved for a bump size of 100 μm. The remaining power busses are supplied via a flat kapton cable glued on top of the readout chips. On two cells per chip, a p-well underneath the input pad defines a 30 fF calibration capacitance. Because of the large number of pixels and the expected low occupancy, a selective readout scheme was implemented on the chip [17], identifying and outputting the addresses of the hit pixels. The connections between the detector substrate and the flat kapton cable, and then to the long kapton cable which is connected to the repeater electronics, are made with wire bonding. The assembly of a pixel plaquette is illustrated in figure 4a.

The ministrip crowns each contain 6 pairs of back-to-back plaquettes. As for the barrel, MX6 chips were used, glued to 300 μm thick BeO hybrids. Due to the lack of space the hybrids are glued directly on top of the single-sided plaquettes. A ceramic or glass fan-in was used to match the 50 μm electronics pitch with the 200 μm readout one. The back-to-back detectors are rotated by 90° with respect to each other, to give a two dimensional readout. The implanted strips have an angle of 2° with respect to the edge of the detector, so by rotating modules in adjacent crowns a 4° stereo angle is created between the strips, helping the pattern recognition. The assembly of a back-to-back ministrip component is illustrated in figure 4b.

5   Readout Electronics

The repeaters are multilayer printed circuit boards mounted in the form of rows of semicircular discs at the ends of the Silicon Tracker. They contain buffers, control circuits and power lines, and communicate with the readout systems in the barracks approximately 20 m away.

Characteristics of modules/crowns	Barrel			VFT		
	Outer	Inner	Closer	Pixel 1	Pixel 2	Ministrip
# modules/crowns	24	20	24	4	4	8
# plaquettes	16	8	4	19	19	12
sensitive area (cm^2)	292	208	103	189	189	324
dimensions (cm)	55.9×3.4	55.5×3.4	36.0×2.1	$r_{min} = 6.9$ $r_{max} = 8.4$	$r_{min} = 7.5$ $r_{max} = 11.2$	$r_{min} = 6.8$ $r_{max} = 11.2$
support material	kevlar + carbon	kevlar +carbon	kevlar +carbon	Aluminium	Aluminium	Aluminium
chip	TRIPLEX	MX6	MX6	SP8	SP8	MX6
power/chip (W)	0.2	0.2	0.2	0.017	0.017	0.2
# chips	20	20	12	304	304	24
% overlap	12	13	15	37	12	15
rad tolerance (krad)	50	50	50	10	10	50
angle to z-axis (deg)	0	0	0	12	32	49

Table 2: Characteristics of modules and crowns. Sensitive area counts $R\phi$ and Rz sides for cases of double-sided detectors. The VFT detectors are supported with ceramics in the case of the pixels, and aluminium plates in the case of the ministrips.
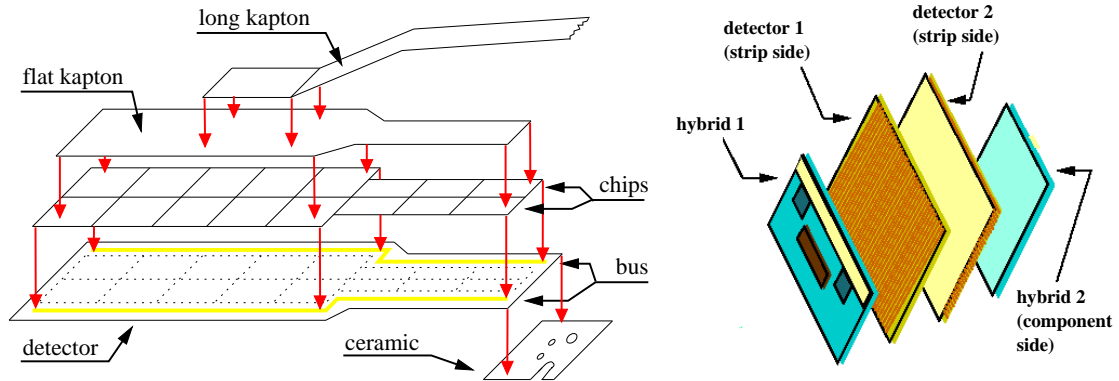

Figure 4: Assembly of the pixel (left side) and ministrip (right side) components of the VFT crowns.

The readout electronics of the barrel and ministrip parts of the Silicon Tracker are similar enough to be steered and read out by a common system. At each second level DELPHI trigger 174080 analogue values from the barrel and ministrip parts of the Silicon Tracker are presented to the readout system. These data are analysed in real time by an on-line computer farm made of 128 DSP56001 Digital Signal Processors. Each DSP is conveniently assigned to one, two or four detector modules and receives between 1280 and 1536 analogue readouts for the analysis. For every DSP the readout is performed in a serial form at the speed of 1 MHz. As all modules are read out in parallel, it takes about 1.6 ms to read out all the strip detectors. Each DSP measures the pedestal and noise of every channel by averaging data over several events. The channels with significant signal are chosen, and signals on adjacent channels are correlated to match the typical charge spread patterns. The DSP's together with the digitization electronics are built into SIROCCO FASTBUS modules [18], which accommodate two DSP's each. The zero-suppressed data are collected from these modules by a standard DELPHI readout processor and later are joined to the common data stream. The suppression ratio achieved is of the order of 5/1000.

The pixel readout system consists of 16 repeaters read out in parallel by the same number of FASTBUS readout units. The readout units themselves are read sequentially by a FASTBUS crate processor which combines the data stream. A custom designed card provides all necessary timing signals for the SP8 front-end chips [19]. The 16 front-end chips of one plaquette are addressed sequentially and accessed separately one by one. This allows the skipping of malfunctioning chips. With each second level trigger, the readout is started and all timing and clocking signals are activated. The sparse data scan readout in the front-end chips selects the addresses of hit pixels only and transfers them to the crate processor with a 5 MHz clock. The total readout time for a full repeater with 160 front-end chips is typically 1.5 ms, including all bus transfer. A small fraction of pixels are systematically noisy. The total number depends on the threshold settings, and is shown in figure 5 for a range of settings. The crate processor supresses these noisy pixels during acquisition time with the use of a mask which is set in advance using calibration run data. This mask is updated every few months and in case of major changes in the detector settings. The sparse data scan and the noisy pixel suppression together reduce the event size considerably with a typical event size being a few hundred pixels. This number is dominated by the remaining noisy pixels, which are flagged by the online monitoring and later removed off-line (see section 7.2.2).

6   Mechanics

6.1   Mechanical Design

The principal challenges which had to be overcome for the mechanical design were as follows:

- Limited space is available (see figure 7). The space constraints are provided by the 116 mm inner radius of the Inner Detector and the 56.5 mm external radius of the flange connecting the different sections of the beam pipe.

- The structure must be able to be installed inside DELPHI, which limits the total length of the detector to 1050 mm.
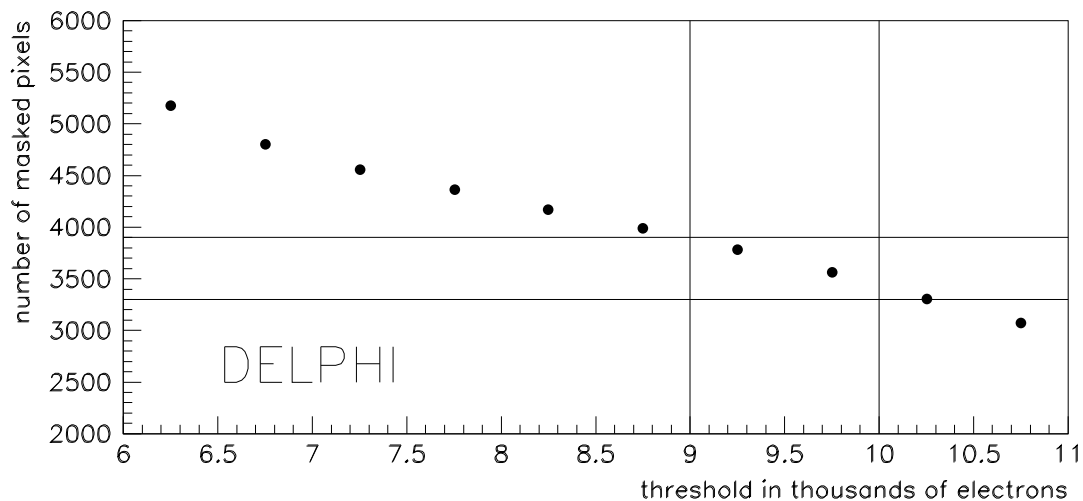
Figure 5: Number of masked pixels as a function of the discriminator threshold for the 1997 detector configuration.

- The Silicon Tracker including the detectors and repeater electronics is 1033 mm long. Within this there are modules which can be as long as 50 cm, mounted in parallel with much shorter modules. The mechanical design must be sufficiently rigid to support all components and suffer as little stress as possible from the varying deformations of the different components with changes of temperature, humidity, etc. At the same time, the extra support material must be kept to a minimum, so as to maintain the previous performance for the $R\phi$ impact parameter resolution in the barrel section.

- The mechanics must be able to re-use all double-sided modules from the previous detector, and accommodate the design accordingly.

6.2 Support Structures

Figure 6 shows diagrammatically a cross section of the modules and supports for one quadrant of the detector. The barrel support consists of light aluminium endrings joined by carbon-honeycomb half cylinders [20]. The Inner and Outer layers are screwed to either side of this endring. The Closer layer has its own endring, which is connected to the barrel via an intermediate composite piece, which also serves to support the internal pixel layer. The thermal expansion coefficients between the components are matched to reduce mechanical stress [21]. The arrangement of the barrel detectors on the endrings is illustrated in figure 7. It can be seen that in order to fit into the space, the support beams on the Outer layer are glued to alternate sides of the modules. An adaptor piece connects the barrel to the forward cylinders. The forward cylinders support 3 crowns of VFT detectors, and also serve to route the kapton cables towards the repeaters. The cabling is arranged in such a manner that using a rotating jig it is possible to mount each section of the detector together with its cabling and repeaters. The resulting structure (see figure 8) maintains the amount of material in the barrel at a similar level to the

1994-95 Vertex Detector, and moves forward material to significantly lower polar angles than previously.

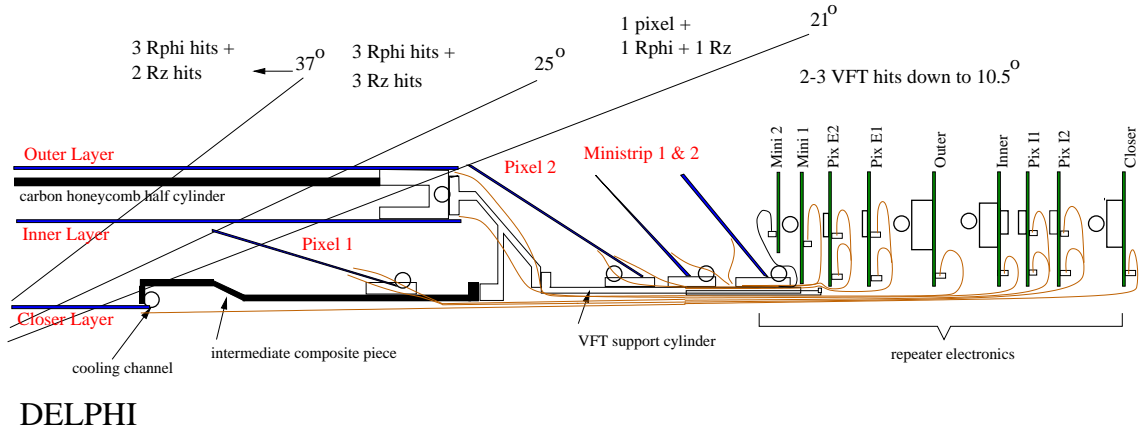A photograph of part of the detector can be seen in figure 9.

Figure 6: Cross section of one quadrant of the Silicon Tracker for z>10cm

6.3 Cooling Considerations

The Silicon Tracker as a whole dissipates about 400 W in an almost completely confined space. In order to remove the heat, a system of cooling with water at 20°C was chosen. The water is delivered to each section of the detector in 0.5 mm thick aluminium tubes with an internal diameter of 3.5 mm. The geometry of the cooling system is based on mechanical considerations and the different power characteristics of each section. In the barrel, the greatest amount of power is developed in the Inner and Outer layers, which have a total of 880 chips dissipating 0.2 W each. These layers are cooled with one tube per quarter. The shorter Closer layer is cooled in parallel, to avoid mechanical stresses due to temperature differences between the layers. The heat transfer between the cooling tubes and the hybrids is optimised with the use of heat paste[6] between all connections. Laboratory tests showed gradients of 4°C for the Inner and Outer hybrids, and a maximum of 6°C for the Closer layer, which has less contact with the endrings. For the pixel detectors, the power dissipation is about 40 W, however the electronics are not localised on the hybrids but distributed over the detector. Here, the cooling functions by both conduction and convection, and the maximum gradients observed can be as high as 12°C. The pixel and ministrip crowns are also cooled in parallel, as well as the repeater electronics, which are cooled with one tube per quarter looping through 5 of the 9 repeater cards.

The cooling is operated on a siphoning principle, with the resultant underpressure protecting the detector from leaks in the system. The water pump used[7] is driven by pressurised air, so there is no heat flow into the system, and the water is cooled by a system of fridges. Problems of algae developing have been avoided with the use of

---

[6]supplied by SCHAFFNER, 5, Rue Michel Carre, 95100 Argenteuil, France
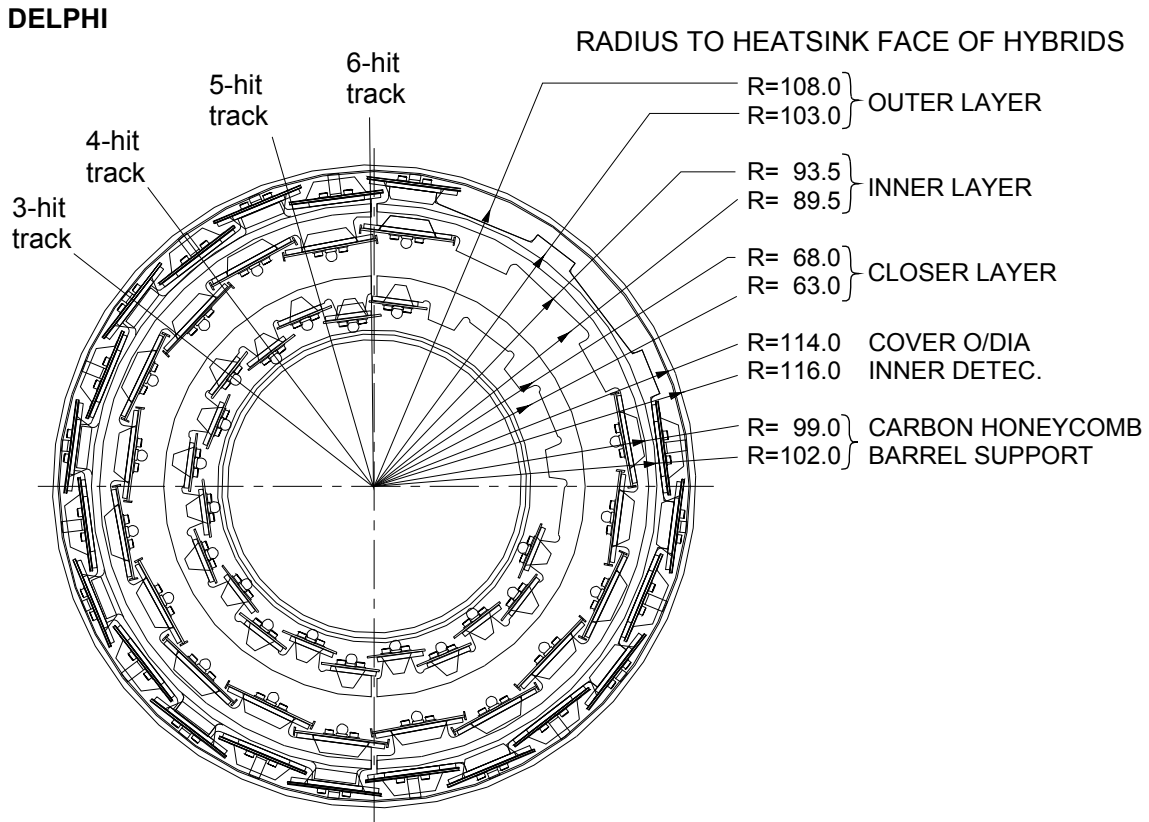[7]supplied by YAMADA EUROPE, Topaasstraat, 7554 TH Hengelo, The Netherlands

Figure 7: Cross section of the Silicon Tracker showing the aluminium support rings of the Closer, Inner and Outer layers with the shape of the modules including the hybrids overlaid. There is a high degree of overlap in all layers, particularly the Closer layer which has roughly 15% overlap. The Inner layer has 20 modules only, as these modules come from the Outer layer of the 1994-95 Vertex Detector and previously formed a ring of 24 modules at higher radius. Spacers are screwed onto the Outer module hybrids to support the cover, which is made from 900 μm thick woven glass fibre with epoxy. The interior cover is supported with screws in 6 Closer layer hybrids. It is made from 1 mm thick Rohacel foam, with a 30 μm thick aluminium shield. The spheres used in the survey (see Section 7.3.1) are shown for the Closer and Inner layers. All spheres are removed before the installation into DELPHI. Note the overlaps between the top and bottom detectors, spanning the space where there is a gap in the support mechanics.

DELPHI
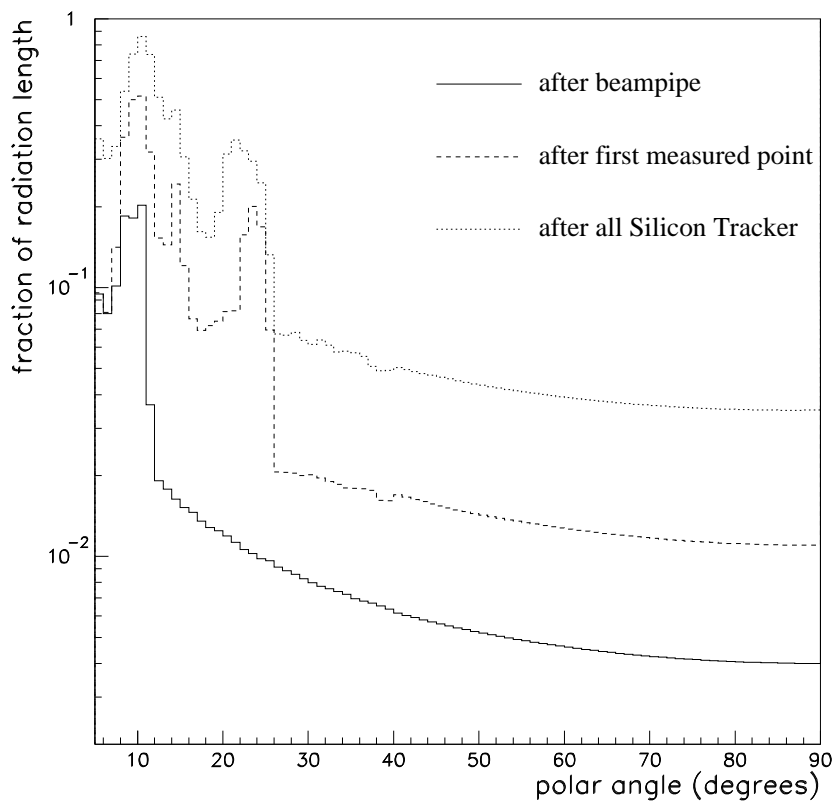

Figure 8: Material of the Silicon Tracker as traversed by particles at polar angles θ. The most important term for the impact parameter distribution is represented by the dashed line, which shows the material just after the first measured point. The values at $\theta = 90°$ are 0.4%, 1.1% and 3.5% for points after the beam pipe, the first measured point and the whole Silicon Tracker respectively.
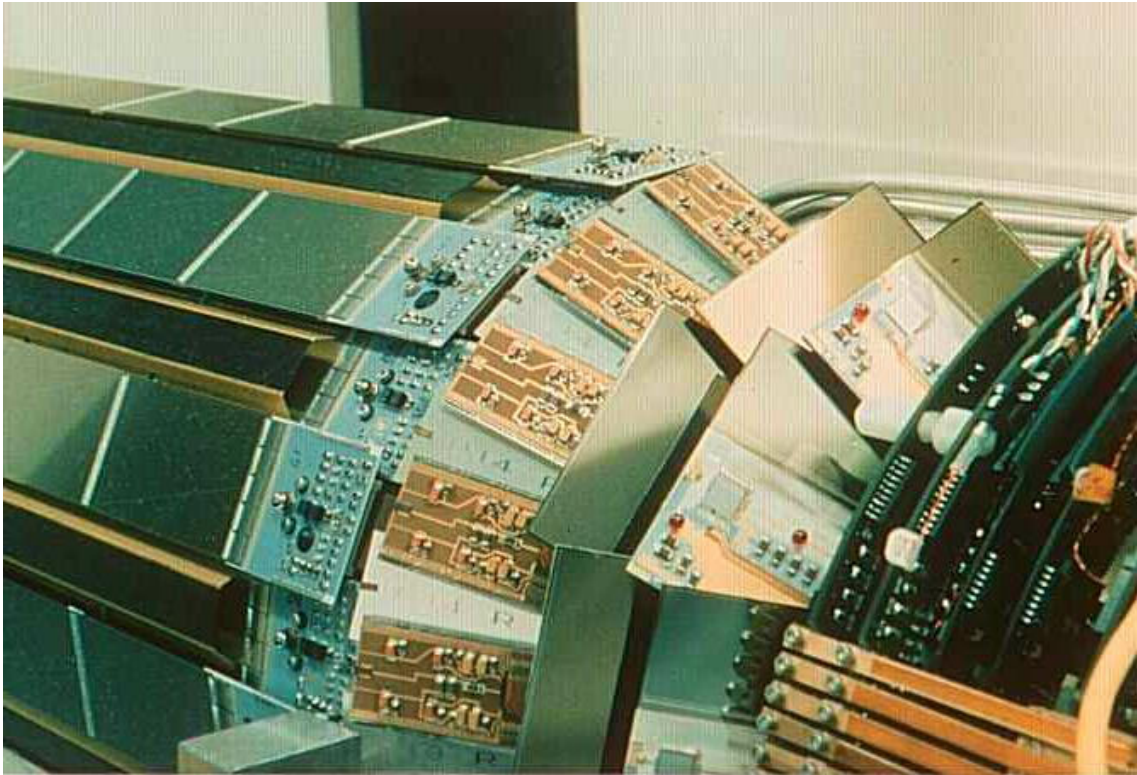
Figure 9: Photograph of part of the detector showing from left to right Rz detectors of the Outer layer with their hybrids, the second pixel layer, two ministrip layers and part of the repeater electronics.

Kemazur 1636[8]. The system has a total of 20 independent cooling tubes, and bifurcation of the tubes inside the detector is avoided, except for short sections in the VFT crowns. This means that sections can be operated independently, and allows for a total water flow of 16 l/min.

6.4 Installation

The detector is installed inside DELPHI with the beam pipe already in place. The weight of the detector is supported on carbon fibre rails via two aluminium skates per half shell. The skates are 3 mm thick at the place where they pass between the barrel detectors and the second pixel layer, and widen to 8 mm at the foot. In the horizontal plane there are also side skate supports, made from 2 mm thick aluminum, with teflon coated heads, which rest on side rails. Extra skates support the repeater electronics. In order to pass the support ring of the beampipe the rails are pulled apart, separating the two halves. The halves must be reassembled before entering the centre of DELPHI, which limits the total length of the detector to 1050 mm. The detector is pulled into DELPHI with cords, and the two halves (each weighing around 3.5 kg) are brought together with a precision of 100 μm using locating pins mounted in the aluminium endring of the barrel. A complete mockup of the centre of DELPHI was built and test installations performed with the true Silicon Tracker.

7 Detector Performance

7.1 Real Time Control of the Detector

7.1.1 Operational Control

Stable and safe operation is a critical issue for the running of the Silicon Tracker. There is an automated response to changes in the data taking conditions or possible misbehaviours of the detector, running within the framework of the general DELPHI slow controls system [22]. From the safety point of view the temperature of the detector is the most critical parameter. This is monitored with the use of 44 PT100 platinum thermometers[9], placed at the entry and exit of various parts of the cooling system. In the case of the pixels some are mounted on the detectors themselves. The temperature variations seen on the inlet and outlet of the cooling are between 4°C and 7°C and are stable to 0.1°C. Thresholds are set both in software and hardware to check for failures in the cooling system. Other parameters, such as bias voltages and currents, low voltages to electronic drivers and ambient humidity, are also continuously recorded.

For the pixels a CAEN[10] controller supervises power supplies and threshold settings. A procedure was developed to detect and to react to an anomalous number of hit pixels, associated to either a high background or to a misbehaving chip. It is necessary to protect the detector against accidental very high occupancies because the power consumption of a cell connected to a hit pixel increases by a factor of about 10. If the required power exceeds the supply characteristics the detector may then trip off, leading to a jump in

---

[8]produced by Degremont-Erpac, 69263 LYON CEDEX 09, France
[9]from MINCO Products Inc., Minneapolis, Minnesota, USA
[10]Costruzioni Apparecchiature Elettroniche Nucleari S.p.A.,Via Vetraia, 11, I-55049 Viareggi, Italy

temperature of around 12°C, affecting badly the detector stability. A typical situation where this can arise is during the LEP injection, when the occupancy can be up to more than 2 orders of magnitude greater than nominal. When the occupancies are abnormally high the crate processor supervising the data acquisition notifies the slow control system, which raises the thresholds [23]. In addition, for the special period of LEP injection when the backgrounds are expected to be high, the discriminator thresholds are always automatically raised.

7.1.2 Monitoring Data Quality

Online data quality checking is essential for commissioning the detector and for fast feed-back during LEP physics conditions. The Silicon Tracker monitor program [24] reads the data stream of the entire detector, working within the environment of the DELPHI online monitoring system [25]. The routines can quickly detect dead, noisy or inefficient modules. A simplified track search has been implemented for the barrel detector. An online calculation of the residuals between tracks and hits gives information on the stability of the layers. For the pixel detector the occupancy of the modules supplies information on the threshold settings and the quality of the noisy pixel suppression mask.

Trace plots document the development of several quantities as a function of time. As an example, figure 10 shows residuals as measured online in 1996 for the Outer layer of the barrel detector. The LEP high energy periods at $\sqrt{s} = 161$ GeV and 172 GeV can be distinguished, separated by the summer break to install further cavities in LEP.
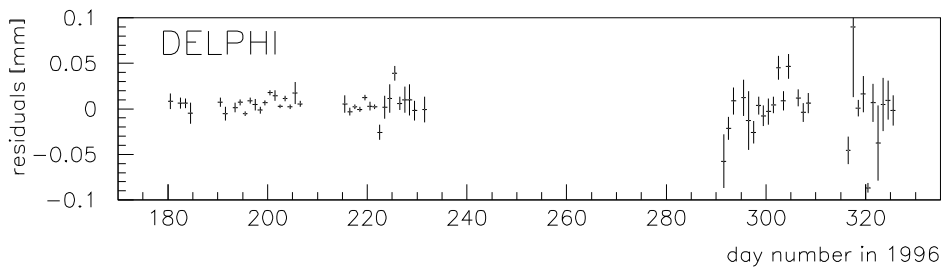

Figure 10: Trace plot of online calculated track residuals in the Outer layer of the barrel detector.

7.2 Noise and Efficiency

7.2.1 Signal over Noise of Strip detectors

Figure 11 gives a summary of the most probable signal over noise (S/N) values for the minimum track length in the silicon shown as a function of the strip length seen by the amplifier. Due to the flipped modules on the Closer and the Inner layers one can

distinguish, on each side of the module, between the $R\phi$ and Rz signals. The highest S/N value is measured for the ministrip detectors, which have relatively short strips. Note that the strip length is only one of several sources of noise affecting the S/N level. Other sources could be inter-strip capacitances depending on the detector pitches, detector current, capacitances between metal layers for the double-metal layer detectors, noise from the voltage supply or charge loss effects from intermediate strips to the second metal layer. The noise performance of the detectors without n-side readout is well described by an offset and a linear capacitance dependence taking into account the length of the strips and routing lines. The additional n implants cause an extra noise contribution which dominates the other contributions (for other discussions see [9, 26]).
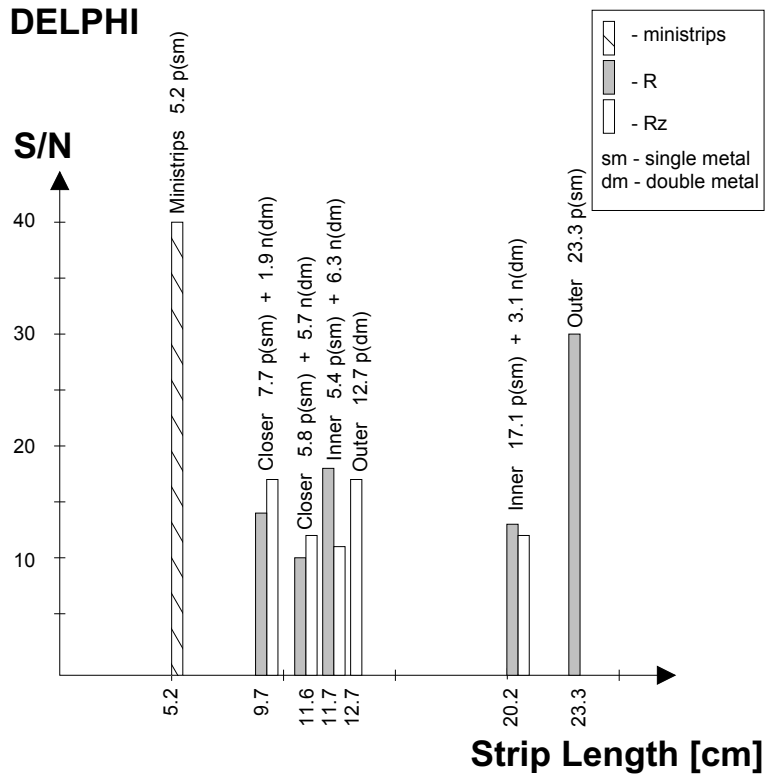

Figure 11: Signal over noise performance of the strip detectors. For each measurement the corresponding length of p and n strips connected to the amplifier is shown, and it is indicated if a double-metal layer is used. The number shown is the most probable value of the S/N.

7.2.2   Pixel Noise

The threshold settings for the pixel detector are placed at a level where the expected sensitivity to charged particles is 99%. The level of systematically noisy pixels for this threshold setting is around 0.3%, as can be seen in figure 5. Most of the noisy pixels are removed by masking in the crate processor, and the remaining ones, defined as those which respond to more than 1% of triggers, are flagged and removed off-line. Figure 12 shows day by day the mean number of noisy pixels which were flagged during the runs

at $\sqrt{s} = 172$ GeV. With the suppression mask unchanged, their number rises slightly in time. On day 324 a new mask was applied.
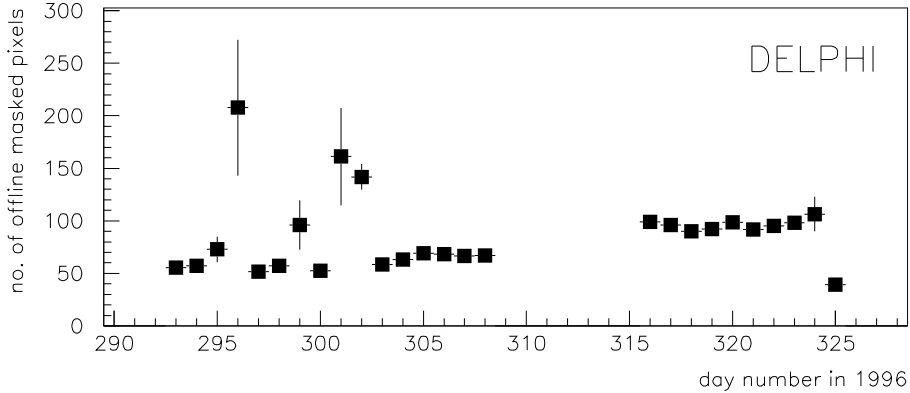

Figure 12: Trace plot of the mean number of pixels flagged as being noisy in addition to those masked in the crate processor. They are removed from the data offline.

After the noisy pixel removal, the hits which remain originate from particles traversing the detector and from random noise. The number of pixel hits is shown in figure 13 for three classes of events. Hadronic events, where some tracks pass through the forward region, have a mean number of pixel hits of about 4.5. Background events, which are triggered events with no tracks pointing to the primary vertex, include beam gas interactions with large showers at small angle and result in a tail extending to very large numbers of hits. Such events become more prevalent at higher energies. A class of events was also selected with just two charged tracks reconstructed in the barrel. These events should produce no physics background in the forward region, and the mean number of pixel hits places an upper estimate on the random noise of 0.5 ppm.

7.2.3 Efficiency

The efficiency of the barrel part was studied using good quality tracks from hadronic events. The tracks were required to have a minimum momentum of 1 GeV/c, be reconstructed with a minimum number of track elements from other detectors, and lie within the polar angle range $27° < \theta < 153°$. Tracks with a hit in two layers were taken and extrapolated to the third layer, where a hit was searched for. An identical analysis was performed on a Monte Carlo sample simulated with a fully efficient Silicon Tracker, and all results were normalised to this. Excluding dead and noisy detectors, the chance of finding the $R\phi$ hit associated with a track for the 1996 data was found to be 93.5%, 98% and 99% for the Closer, Inner and Outer layers respectively, and 99.4% of tracks have at least two associated $R\phi$ hits. The problematic detectors made up a total of 10%, 2% and
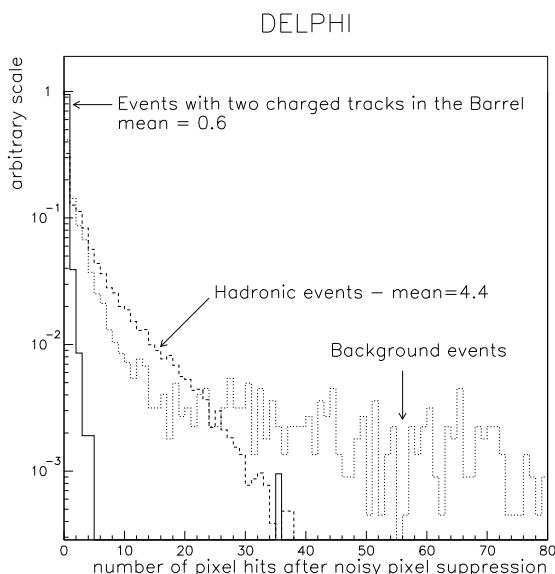
21

Figure 13: Mean number of pixels per event for hadronic events, background events, and events with two charged tracks only in the barrel. The data are taken from the 1997 Z^o running period. The normalisation is arbitrary.

2% in the three layers, and had a lower average efficiency of around 60%. The probability of finding the z hit associated with a track which has an $R\phi$ hit associated in the same layer was found to be 96% for the Closer layer and 98% for the Outer layer.

The efficiency of the pixels was studied using tracks which pass through a region where neighbouring plaquettes overlap and have at least one hit in a silicon layer other than the one being studied. If a track registers a hit in one plaquette, a second hit is searched for around a 3σ window in the neighbouring plaquette. Figure 14a shows the average efficiency measured in each pixel crown using this technique. It was possible to measure the efficiency for 130 plaquettes. Of the remaining plaquettes, 16 were dead or partially dead, and the remaining 6 were overlapping with bad detectors or did not have a good enough alignment. The average efficiency excluding bad plaquettes was 96.6%.

The efficiency for the ministrip part of the detector is determined using electrons from the dominant process of t-channel small angle Bhabha scattering. The electrons are required to be tagged by the shower signature in the forward electromagnetic calorimeter, and have at least one hit in a silicon layer other than the one being studied. A set of 18000 Bhabha events was selected for the analysis. When a track registers a hit in the overlap region between two plaquettes a hit was searched for in a 3σ window in the neighbouring plaquette. The results of this measurement are shown in figure 14b where the efficiency based on 90 ministrip plaquettes is shown for each ministrip crown. An average efficiency of 98.5% was measured. The remaining 6 dead plaquettes were excluded from the measurement.
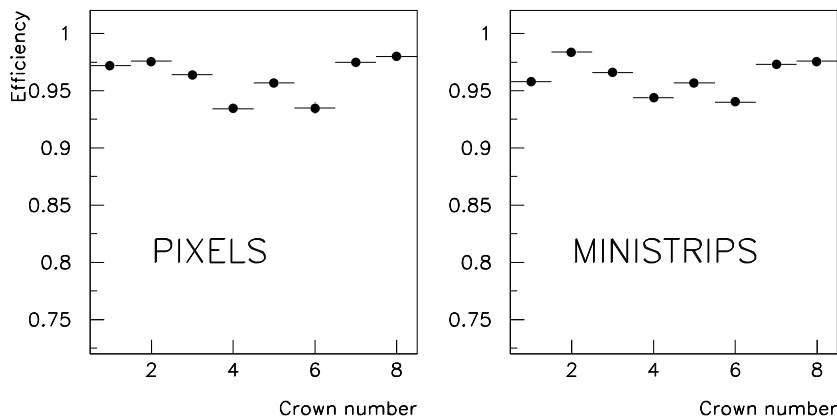
Figure 14: Efficiency for the pixel and ministrip crowns as measured in the 1997 data using tracks (see text). The average quoted efficiencies do not take into account dead modules.

7.3 Alignment

The Silicon Tracker is the basis of alignment in DELPHI. To avoid propagation of errors from the other tracking detectors, the only measurement taken from outside the Silicon Tracker when performing the alignment is the momentum of the tracks.

The alignment of the full Silicon Tracker is performed in four steps.

The first one consists of an optical and mechanical survey of the individual components and of the whole structure of each half-shell. Being made before the installation inside DELPHI, the survey gives no information on the relative position of the two half-shells. Also the geometry of either half-shell after installation might slightly differ from the results of the survey, due to possible deformations of the mechanical structure.

The second step uses cosmic tracks to commission the detector before the start of LEP running and to make a rough prealignment of the two half-shells with respect to each other and to the other tracking detectors of DELPHI.

The last two steps, final alignment of the barrel and of the VFT, uses tracks from e^+e^- collisions, to perform 4 tasks: parametrisation and correction of the mechanical deformations, refinement of the survey for each half-shell, relative alignment of the two half-shells and external alignment of the whole Silicon Tracker. The alignment procedure for the the barrel is similar to that used for the 1994-95 Vertex Detector, which has been described in detail elsewhere [27].

7.3.1 Survey of the Silicon Tracker

The survey stage [28] is different for the different detector components and it requires both optical and mechanical measurements. Barrel and ministrip modules are individually

23

measured by a camera[11] mounted on the same 3D machine[12] used for the mechanical survey. This measurement provides the position of all strips on either side of a module with respect to high precision reference spheres fitted onto the hybrids.

After assembling all modules into half-shells and half crowns, a 3D survey of detector layers and reference spheres is made with a high precision touching probe system, which provides the relative positions of all modules within one substructure.

The pixel detectors are surveyed in two steps. After the chips are bump-bonded and the ceramic support is glued to the detector, the two-dimensional position of the external detector corners and the ceramic are determined with a microscope with respect to pads close to the detector corners. These pads have a well known position on the detector mask and define the position of the pixel array. They are chosen as a reference as they remain visible during the assembly. The kapton cables are then attached and the tested module mounted on the support. Its position, given by the location of the two corners plus the measurement of the module's plane, is related to that of three spheres mounted on the support. After all modules are mounted, the VFT crowns are joined to the barrel support and the positions of the spheres with respect to the barrel are measured.

The intrinsic accuracy of the survey is below 10 μm, but the overall precision of the description of the actual detector in DELPHI is limited by deformations which occur after the survey. The main kinds of coherent deformations which can be expected are:

- There may be a twist of the barrel around the z axis or a tilt of the barrel endrings which maintains them parallel to each other (as the distance between the endrings is fixed by the module length). The effect of such distortions on the VFT crowns is illustrated in figure 15.

- The pixel detectors are mechanically bound to the support at one end only, and experiencing the pressure of the kapton cable may bend in polar angle. This can affect the local z coordinate by up to a few hundred microns.

- The modules in the barrel may develop a bowing relative to the survey. The effect is small for the Closer layer but its amplitude might be as large as large as 150 μm in the middle of a module of the Inner or Outer layer. This effect is related to stress during installation and to variations in humidity.

The study of the actual distortions of the Silicon Tracker structure after installation into DELPHI is performed with reconstructed tracks as described in the next sections.

7.3.2 Alignment of the Barrel

The Barrel alignment procedure uses three following classes of tracks: $e^+e^- \rightarrow \mu^+\mu^-$ events at the Z^0 pole, tracks passing through the the overlap regions of two adjacent modules and tracks passing through only one module of each layer. The only information taken from the other tracking detectors of DELPHI is the track momentum.

The survey is used as a starting point, and before the alignment begins, the following effects are parametrised and corrected for:

---

[11]Mondo Machine Developments Ltd., Leicester, UK.
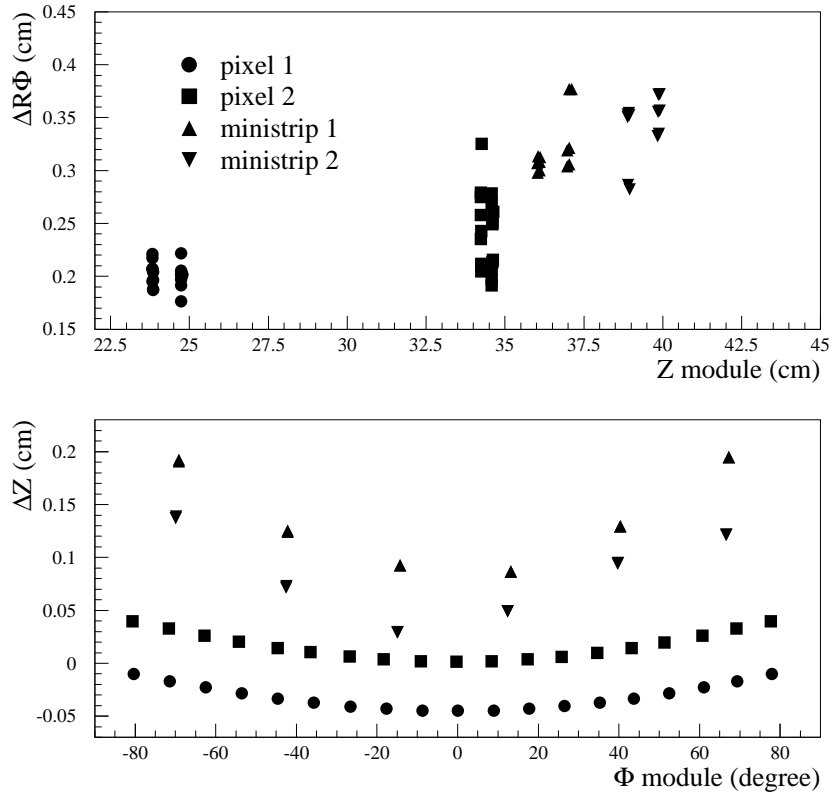[12]POLI S.p.A., Varallo Sesia, Italy.

Figure 15: Differences between the survey and the final VFT alignment for the fully equipped quarter of 1996; the biggest movements found are a torsion of the structure, visible as an $R\phi$ shift dependent on the z of the layers, and a rotation of the crowns about the vertical axis, which shows up as a systematic dependence of the translation in z on the position of the module.

- It appears that the barycentre of the holes (and electrons) created by a particle crossing a detector and collected by the implant lines does not correspond exactly to the mid-plane of the detector, but are shifted towards the p-side by 10–20 μm. This effect was first established with data from the 1994-95 Vertex Detector [27, 29].

- The shape and amplitude of the bowing mentioned in section 7.3.1 is parametrised using overlap residuals.

- A possible time or fill dependent acolinearity and momentum imbalance of the LEP beams affects the trajectories of the muon pairs at the Z^0 pole used for alignment. Both effects are measured by the LEP machine group.

The alignment procedure then uses tracks through overlaps to align the Outer layer, muon pair tracks to align the Closer layer with respect to the Outer layer, and finally the Inner layer is aligned with respect to the other two layers. The actual procedure deals with 408 degrees of freedom and consists of a complex sequence of elementary steps repeated iteratively [27].

At LEP2 the integrated luminosity delivered at the Z^0 peak is a factor of 50 below that of previous years, resulting in a limited number of muon pairs useful for alignment. The performance of the alignment procedure is hence statistically limited for the impact parameter resolution at large momenta. However in the momentum interval relevant for b hadron decay products the effect is negligible. The lack of dimuon events is partially compensated with the use of cosmic tracks.

As an illustration of what is gained by the internal alignment together with the correction of elastic deformations, figure 16 displays the distribution of the residuals between the two hits of a track passing through the overlap of two adjacent modules, before and after internal alignment, for $R\phi$ hits and for Rz hits.

7.3.3 VFT Alignment

The VFT alignment procedure uses track elements already reconstructed with the use of the other tracking detectors. The procedure optimises the VFT module positions by minimising the χ^2 of tracks refitted over all track elements. The weight of the track in the fit depends on the polar angle and the combination of tracking detectors contributing to the track. In addition, the intrinsic VFT resolution and the constraints from overlapping modules are exploited. The global parameters at the level of each quadrant are determined first, then the individual plaquette parameters are fitted, allowing 6 degrees of freedom per plaquette. The overlap between the first pixel layer and the Barrel Inner layer at $20° < \theta < 25°$ provides the link between the Barrel and the VFT global alignment.

7.4 Alignment Performance

In the barrel, the precision of the alignment can be checked using residuals between overlapping modules, track hit residuals, and impact parameter distributions. The best hit precisions are found in the Outer layer, as these are used as constraints in the alignment procedure. The distributions are shown in figure 17 for the $R\phi$ and Rz projections. Taking the appropriate geometrical factor into account, the hit precision found is 9 μm in the $R\phi$ projection and 11 μm for perpendicular tracks in the Rz projection. The Closer layer
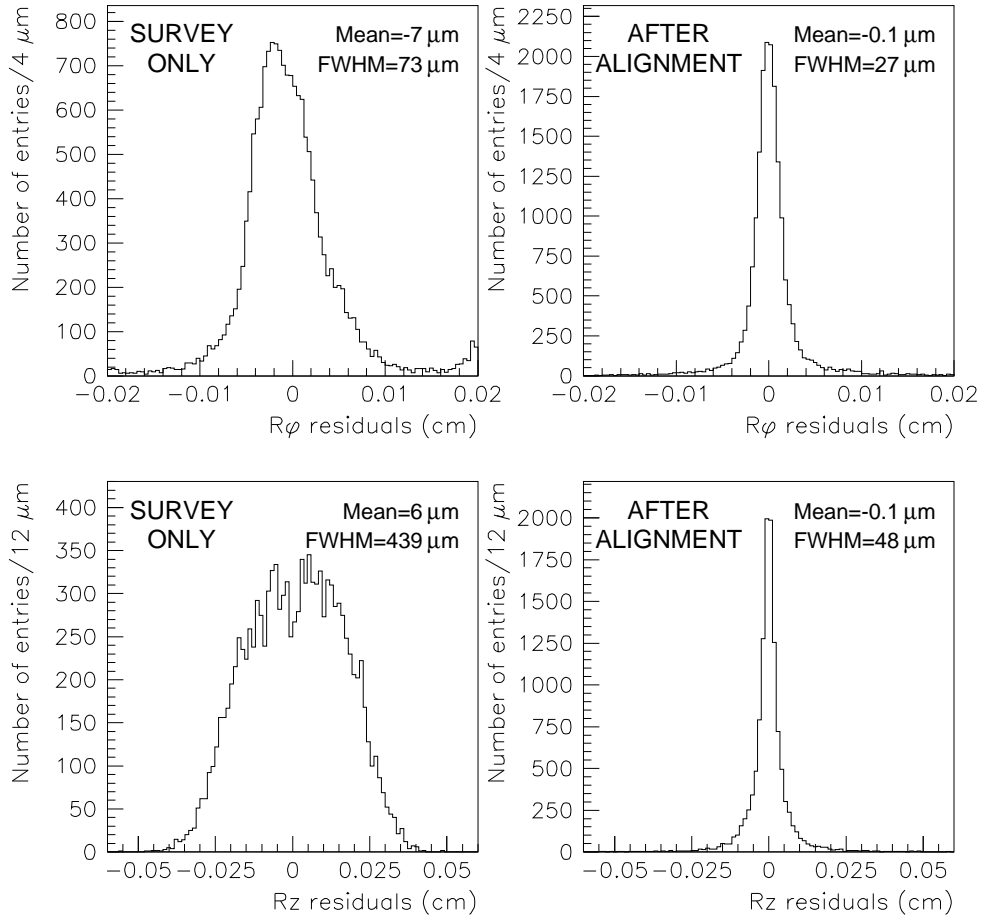
DELPHI

Figure 16: The residuals between two hits associated with tracks passing through the overlaps between modules. $R\phi$ residuals (upper plots) and z residuals (lower plots) are shown for the detector positions obtained from the survey (left side) and given by the final alignment (right side).

shows similar distributions with a hit precision of 11 μm in the $R\phi$ plane and 14 μm in Rz. The excess of these numbers over the Outer layer precision indicates the quality of the alignment. The Inner layer makes a less important contribution to the impact parameter resolution and is important mainly for pattern recognition and redundancy. In $R\phi$ the hit precision in this layer is measured to be 13 μm and in Rz, measured for polar angles below 37° only, is 70 μm in the detector plane.

DELPHI
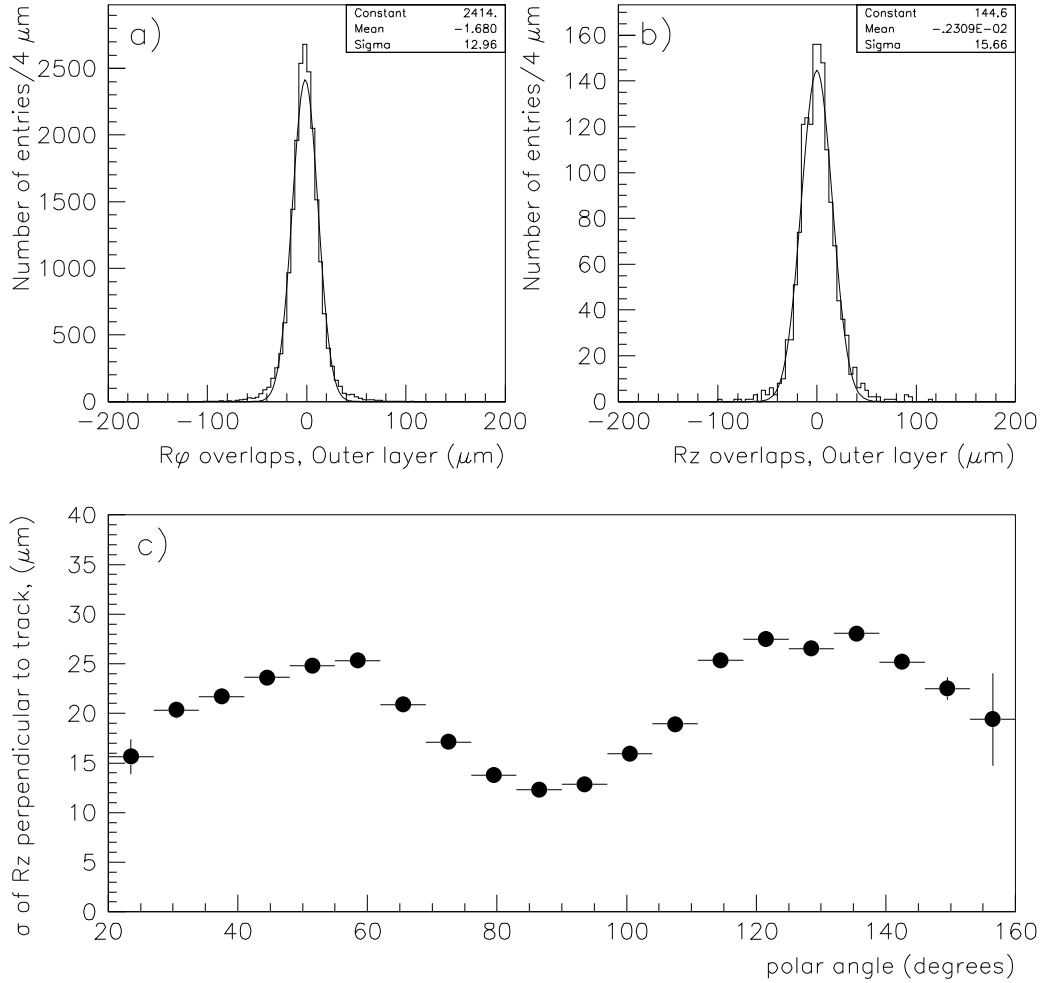
Figure 17: Plots a) and b) show residuals in overlapping detectors of the Outer layer in the $R\phi$ and Rz projections. The width must be divided by $\sqrt{2}$ to obtain the single hit precision. Plot c) shows the Rz precision of hits in the Outer layer in the direction perpendicular to the track.

An independent check of the alignment is provided by the impact parameter resolutions, displayed in figure 18. The top plot shows the impact parameter in $R\phi$ as a function of momentum, and is fitted with the function 28 μm $\oplus$ 71/(p $\sin^{\frac{3}{2}}\theta$) μm, where p is the

28

track momentum in GeV/c. The bottom plot shows the impact parameter resolution in Rz for perpendicular tracks and is fitted with the function $34\ \mu\text{m} \oplus 69/p\ \mu\text{m}$. In both these cases the first term is the asymptotic value and the second term contains the effects of multiple scattering. Taking into account the correct geometrical factors one estimates effective hit precisions of 8 μm and 9 μm in the two coordinates. Figure 18b combines tracks at all theta angles and fits the Rz impact parameter resolution with the function $39\ \mu\text{m} \oplus 75/(p\ \sin^{\frac{5}{2}}\theta)\ \mu\text{m}$.

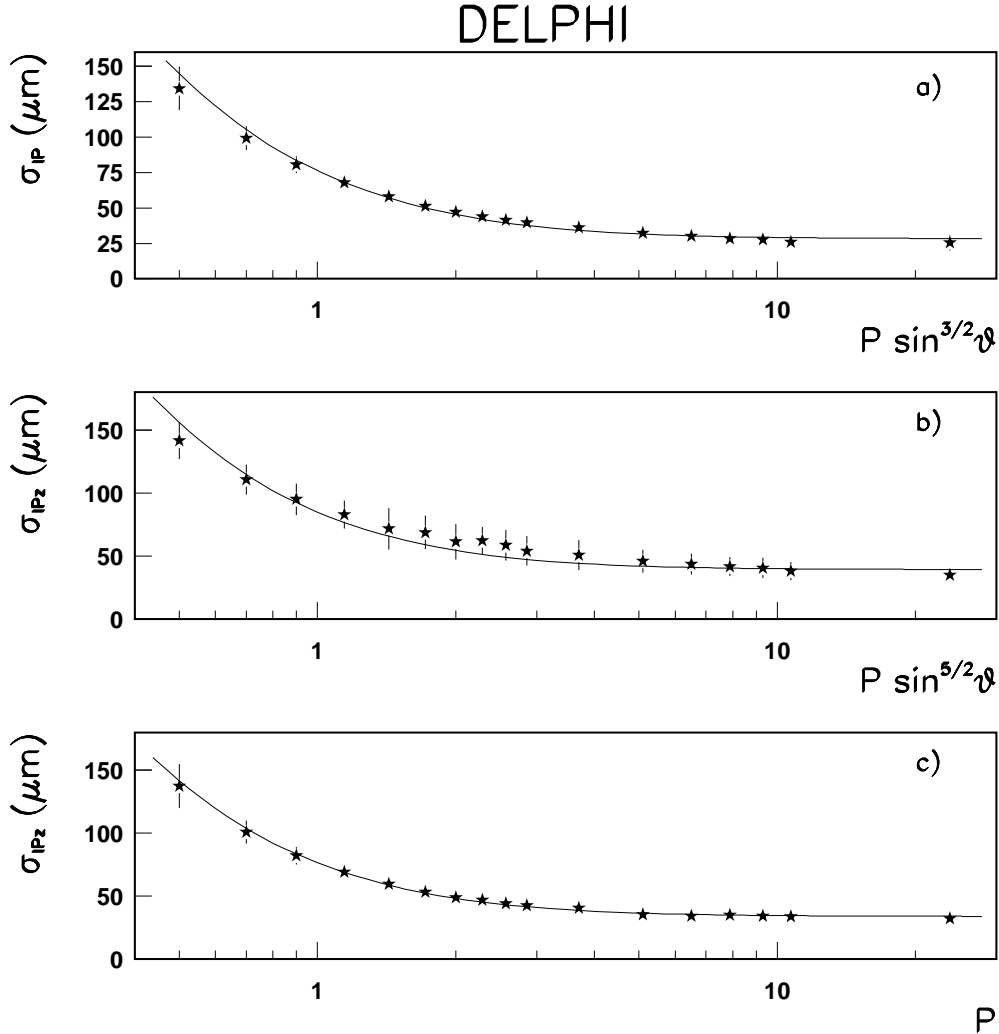
Figure 18: Impact parameter resolutions as a function of momentum, for: a) $R\phi$, b) Rz (all tracks), and c) Rz (perpendicular tracks) projections.

The internal alignment of the VFT is also checked using tracks passing through over-lapping detectors. For the pixels, the expected resolution depends on the cluster size, which is a function of the track incidence angle. Tracks from the primary vertex traverse the first and second pixel layer at incidence angles ψ in the polar direction of 57.5° and

40.5° respectively. The incidence angle in the $R\phi$ direction is close to 90°. The majority of produced clusters are either single hits or double pixel hits split in the polar direction. Neglecting charge diffusion effects, the angular dependence of the single pixel hit rate is given to first order by the following equation:

$$N = (1 - \frac{d}{\Delta}); \qquad d = w \times \tan\psi - \frac{t}{c} \times w \times \sin\psi \tag{1}$$

where w is the thickness of the depletion layer, Δ is the pixel pitch, c is the charge deposited by a minimum ionising particle and the parameter t is given by the detector threshold (about 10ke$^-$ is used). Knowing this rate, a simple geometrical consideration of ionisation charge sharing in the pixel sensitive volume leads to the following expression for the expected detector resolution:

$$\sigma^2(\psi) = \frac{1}{12} \frac{(d^3 + (\Delta - d)^3)}{\Delta} + (\frac{\kappa}{c} \times w \times \sin\psi)^2 \tag{2}$$

Here κ is a parameter describing the effect of charge fluctuations (about 5ke$^-$ is used), and the other symbols are the same as in equation 1. The expected distributions are displayed in figure 19 as a function of ψ. The resolutions in the data are measured in the detector plane for the z_local (polar) direction and the x_local ($R\phi$) direction. The values extracted are overlaid on the prediction. For the x_local points the incidence angle is the same for the pixel I and pixel II layers, and these points are shown together. The measured points are seen to be very close to those predicted by the simple model.

Figure 20 shows the residuals for the ministrip overlaps. The internal hit precision derived from this plot is 30–33 μm, as expected from previous studies [26].

8   Physics Performance

8.1   Performance of b-tagging in 1996 Run

For the Barrel the b-tagging performance of the Silicon Tracker is important for physics analyses. Figure 21 shows the b-tagging efficiency [30] as a function of the polar angle of the event thrust axis. The full line is the performance of the 1994-95 Vertex Detector, which had a 3-layer coverage down to a polar angle of 42° and a Closer layer coverage down to 25°, and the points show the performance in 1996 of the new Silicon Tracker. It can be seen that the new extended barrel maintains the performance of the previous Vertex Detector in the central region, while there is a clear gain in the region between 25° and 42°.

One of the main physics goals of LEP2 is the Higgs search. A good efficiency for the signal and a good background rejection can be reached as shown in figure 22, where the efficiency for an event tag in the region $|cos(\theta)| \leq 0.9$ is shown for ZH, hA, WW events and the QCD background.

8.2   Improvement of Tracking in the VFT Region

The tracking situation in the forward region is considerably different to the barrel part of the Silicon Tracker. A description of the DELPHI tracking detectors may be found in [3]. In the forward the TPC measures only short track elements of particles leaving
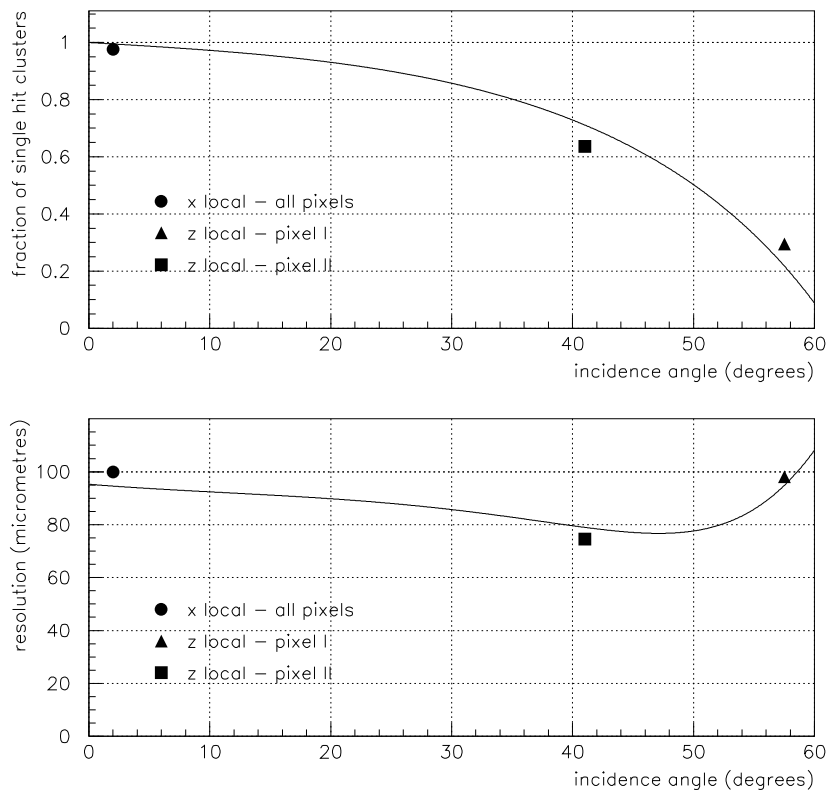
DELPHI

Figure 19: Resolution expected in the pixels as a function of track incidence angle (solid line) shown together with the values measured in the data.
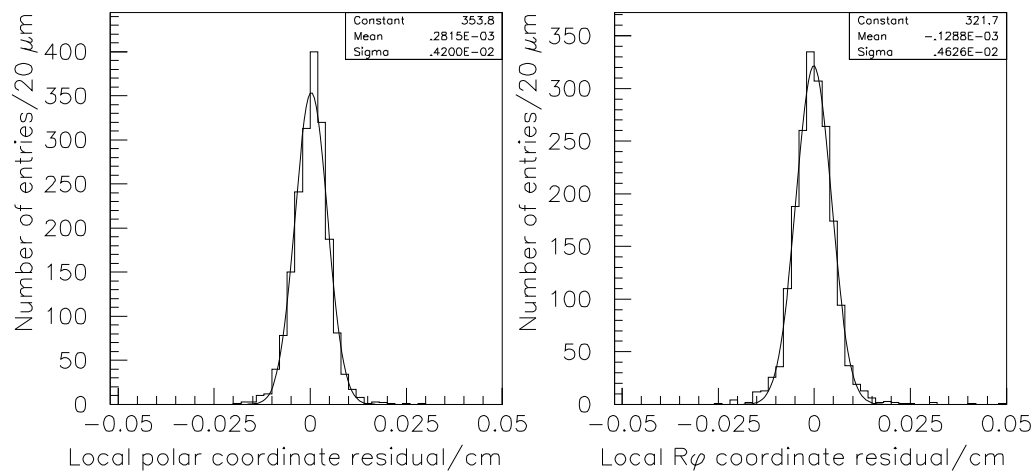
Figure 20: Local alignment residuals for ministrip modules. To derive the internal hit precision the widths must be divided by $\sqrt{2}$.
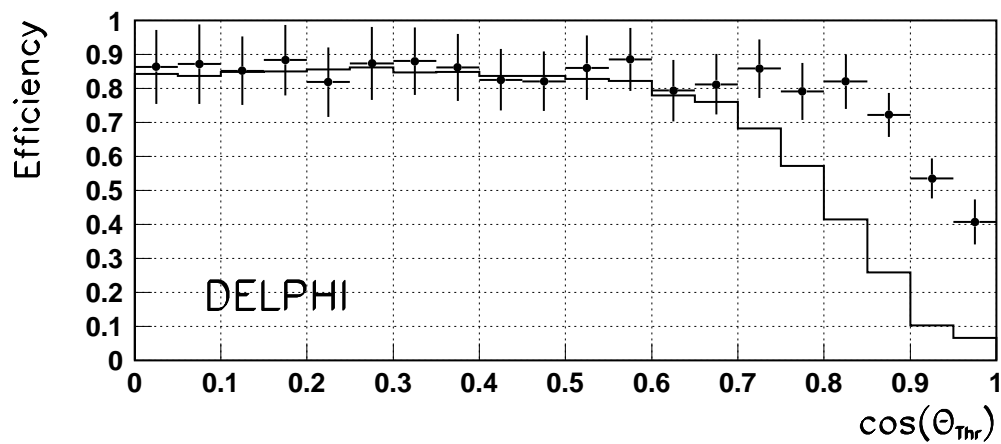

Figure 21: The efficiency versus $cos(\theta_{Thr})$ for the new microvertex detector (points) and the previous shorter one (full line).
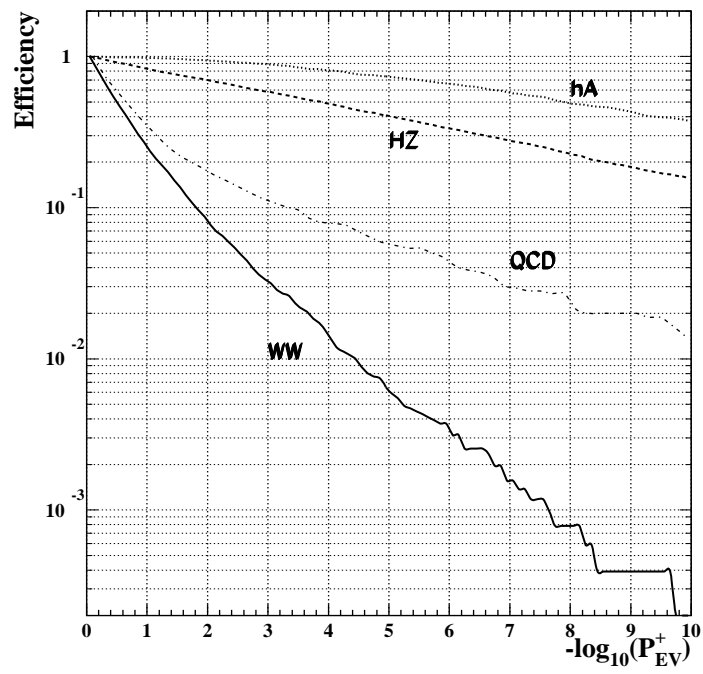
Figure 22: The efficiency for an event tag P_{EV}^+ is shown for hA, ZH, WW events and the QCD background (taken from [31]).
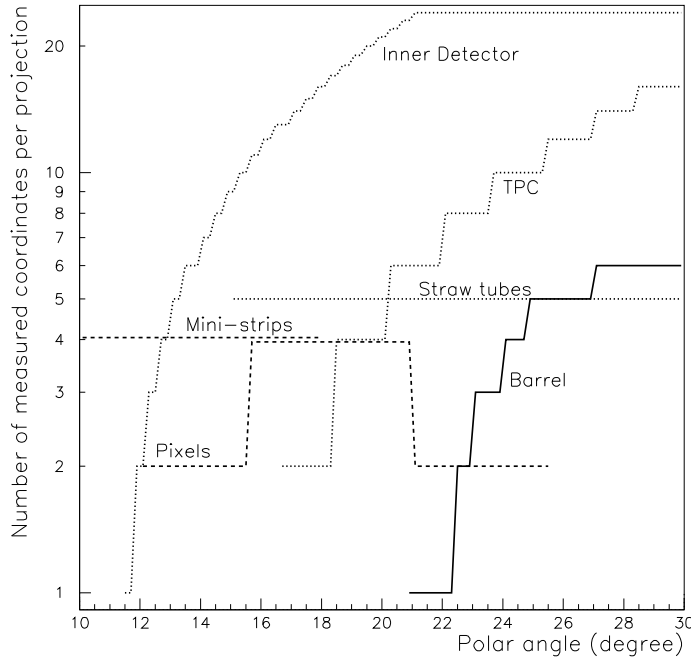
Figure 23: Number of coordinates measured by the innermost tracking detectors shown as a function of polar angle for the forward region. One entry is shown for each $R\phi$ and each Rz measurement. The vertical scale is logarithmic. The detectors shown are the TPC (minimum radius 40 cm), the Inner Detector Jet Chamber ($R\phi$ information, minimum radius 12 cm), the straw tubes ($R\phi$ information, minimum radius 23 cm) and the layers of the Silicon Tracker. The outer tracking detectors not shown in this plot provide measurements at $|z| > 160$cm.

through its endcap, and there are fewer $R\phi$ points provided by the jet chamber of the Inner Detector. Additional tracking information is provided by the forward chambers before and after the Forward RICH and by the measured track elements in the drift tube of the Forward RICH itself. However the track finding efficiency using these chambers alone is limited by interactions in the material in front of them. The situation in the forward region in summarised in figure 23 which shows the number of coordinate points reconstructed by the inner tracking chambers as a function of polar angle. The overlap between the various detectors can be seen, as well as the decreasing importance of the TPC and Inner Detector in the forward.

The VFT space point measurements are fully integrated in the DELPHI reconstruction. The VFT standalone pattern recognition is used to reconstruct track elements pointing to the primary vertex out of multiple hits in the different layers. These elements are used in the global reconstruction as a seed for the track finding. Measurements in the ID are extrapolated to the VFT to pick up the correct track element before extrapolating to the other detectors. The extrapolations may also be improved by constraining the VFT track element to the primary vertex.
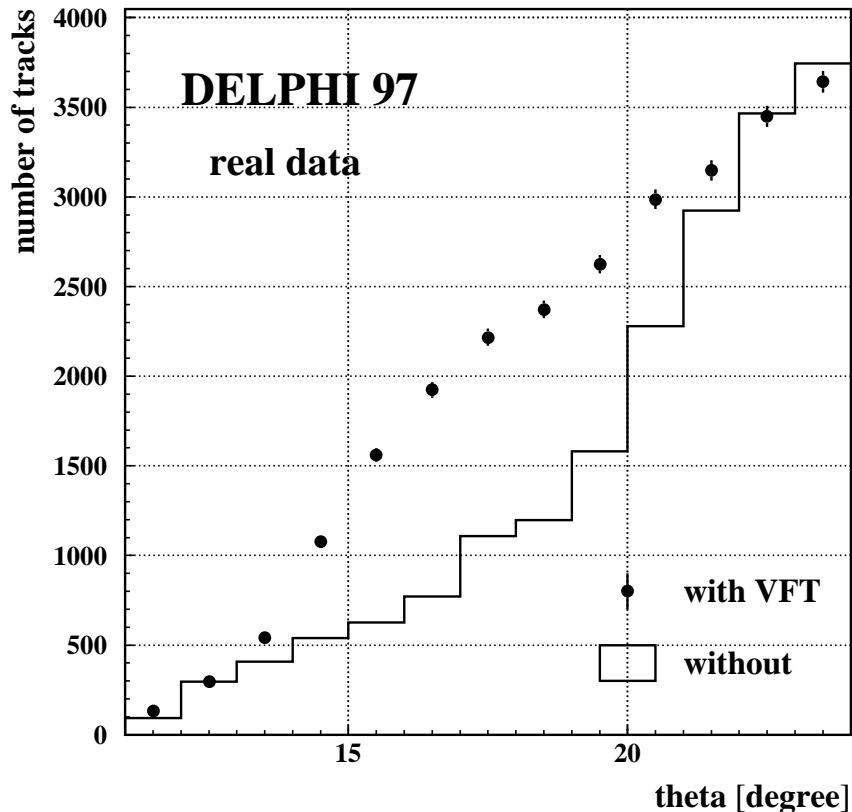
34

Figure 24: Number of reconstructed tracks useful for physics analysis reconstructed with the VFT (dots) and removing the VFT from the tracking (line) shown as a function of polar angle [32].

Figure 24 shows the improvement due to the VFT in the number of tracks reconstructed in the forward region. Simulation studies show that for 91% of the particles crossing the VFT the hits are associated to the tracks, and the purity of the associations is 94%. This compares with a purity of 98% for the Barrel.

9   Conclusions

The final upgrade of the DELPHI Silicon Tracker, to enable DELPHI to meet the physics requirements of LEP2, was completed in 1997 and has accumulated about 70 pb^{-1} of high energy data. The Silicon Tracker contains 888 detecting elements having a total active surface of about 1.6 m^2 of silicon, has 1399808 readout channels and covers polar angles between 11° and 169°. It consists of the Barrel, extending from 21° to 159° and playing the role of vertex detector, and the Very Forward Tracker (VFT) in the form of two silicon endcaps, providing standalone pattern recognition and increasing the track reconstruction efficiency between 11° and 25°.

The Barrel contains 640 AC coupled microstrip silicon detectors, arranged in three

layers at average radii between 6.3 and 10.8 cm. The 149504 electronics channels read signals collected on the strips which give $R\phi$ measurements with a readout pitch of 50 μm and Rz measurements with pitches varying between 42 μm and 176 μm. The material in the sensitive region is kept to a minimum by the use of double-sided detectors, double-metal readout and light mechanics.

Each of the two VFT endcaps contains two layers of silicon pixel detectors and two layers of ministrip detectors. The pixels have dimensions of 330 $\times$ 330 μm^2 and there are 1225728 in total. They are connected to the readout electronics channels using an industrial bump bonding method and their readout is performed by a sparse data scan circuit. The AC coupled ministrip detectors (96 in total, corresponding to 24576 electronics channels) have a strip pitch of 100 μm and a readout pitch of 200 μm.

The complete Silicon Barrel and a large part of the VFT was already in operation during the 1996 data taking at LEP2, and the complete Silicon Tracker was installed in 1997.

Acknowledgements

References

[1] The DELPHI Collaboration, *Proposal for the upgrade of DELPHI in the Forward Region*, CERN/LEPC/92-13/P2 Add2, 16th October 1992.

[2] V.Chabaud et al., *The DELPHI silicon strip microvertex detector with double-sided readout*, Nucl. Instr. and Meth. **A368** (1996) 314.

[3] P. Abreu et al., (DELPHI Collaboration), *Performance of the DELPHI Detector*, Nucl. Instr. and Meth. **A378** (1996) 57.

[4] N.Bingefors et al., *The DELPHI Microvertex detector*, Nucl. Instr. and Meth. **A328** (1993) 447.

[5] P.Chochula *et. al.*, *The Silicon Tracker in the DELPHI Experiment at LEP2*, paper 306 submitted to HEP97, DELPHI 97–121 CONF 103. R.Brenner: *The upgrade of the Vertex Detector to form the central part of the Silicon Tracker in DELPHI*, Nucl. Instr. and Meth. **A386** (1997) 6.
V.Chabaud: *The DELPHI Silicon Tracker - Barrel part*, to be published in the Proceedings of the 5th International Conference on Advanced Technology and Particle Physics, Como, Italy, 7-11 October 1996.

[6] A.Andreazza et al., *The DELPHI Very Forward Tracker for LEP200*, Nucl. Instr. and Meth. **A367** (1995) 198.
Ch.Meroni, *The forward extension of the DELPHI Silicon Tracker*, Proceedings of the fourth International Workshop on Vertex Detectors, June 1995, Ein Gedi Resort, Dead Sea, Israel, p.29.

[7] D.Sauvage et al., *A Pixel Detector for the '95 Upgrade of the DELPHI Micro Vertex Detector*, CPPM - 95-05 and Proceedings of the fourth International Workshop on Vertex Detectors, June 1995, Ein Gedi Resort, Dead Sea, Israel, p. 53.
K.H.Becks et al., *Progress in the construction of the DELPHI pixel detector*, Nucl. Instr. and Meth. **A395** (1997) 398–403
K.H.Becks et al., *The DELPHI pixels* , Nucl. Instr. and Meth. **A386** (1997) 11.

[8] V.Cindro et al., *The design of silicon ministrip detectors for the DELPHI Very Forward Tracker*, Nucl. Phys. B (Proc. Suppl.) **44** (1995) 292.
M.Krammer, *The construction of the DELPHI Very Forward Ministrip Detectors*, Proceedings of the fourth International Workshop on Vertex Detectors, June 1995, Ein Gedi Resort, Dead Sea, Israel, p. 41.
W.Adam et al., *The status of the DELPHI very forward ministrip detector*, Nucl. Instr. and Meth. **A 379** (1996) 401.
W.Adam: *Performance of the DELPHI VFT ministrip detectors*, to be published in the Proceedings of the 5th International Conference on Advanced Technology and Particle Physics, Como, Italy, 7-11 October 1996.

[9] I. Stavitski, *DELPHI vertex detector in 1996*, presented at conference "Frontier detectors for frontier physics", 26-30 May, 1997, Biodola, Italy
P.Collins, *Experience with silicon detectors at the DELPHI experiment, LEP*, Nucl. Instr. and Meth. **A383** (1996) 1.

[10] M. Cohen-Solal and J.C. Clemens, *Electronics for pixel detectors*, Nucl. Instr. and Meth. **A380** (1996) 335.

[11] A. Zalewska, *Conventions for the barrel part of the Delphi Silicon Tracker 1996* , DELPHI note 96–146 MVTX 18, 24 October 1996.

[12] P. Seller et al., Nucl. Instr. and Meth. **A214** (1992) 393.

[13] J.Ardelean et al., *TRIPLEX: An Amplification and Trigger Chip for a Si-strip Microvertex Detector*, internal note of LAL, Orsay.

[14] R.Brenner, C.Eklund, *First Testbench Measurements of the DELPHI Vertex Detector Outer Layer Modules for the 1996 Upgrade*, HU-SEFT RD 1995-04.

[15] P.Collins, *The Alignment and Performance of the DELPHI Double-Sided Vertex Detector*, Proceedings of the fourth International Workshop on Vertex Detectors, June 1995, Ein Gedi Resort, Dead Sea, Israel, p. 13.

[16] L.F. Miller, *Controlled Collapse reflow chip joining*, IBM J. of Res. and Dev. 13, no.3 (1969), 239-250.

[17] J.J. Jaeger et al., *A sparse data scan circuit for pixel detector readout*, IEEE Trans. Nucl. Sc. 41, no.3 (1994), 632-636.

[18] N. Bingefors, M. Burns, *SIROCCO IV : front end readout processor for DELPHI microvertex*, Proceedings of the International Conference on the impact of digital micro-electronics and microprocessors on particle physics, Trieste, Italy ; 28–30 Mar 1988

[19] C. Aubret, J.M. Brunet, B. Courty, L. Guglielmi, G. Tristram, J.P. Turlot, *DELPHI Pixel Detector Readout*, Collège de France, Paris, September 13, 1996, available via WWW:
$http://cdfinfo.in2p3.fr/Experiences/Delphi/VFT/vft.html$

[20] L. Denton, *Distortion Tests made on the DELPHI Barrel Support*, internal RAL memorandum, 8th March 1995.

[21] M.Raymond et al., *Design and manufacture of an accurate composite piece*, CERN 94-07, Proceedings of the International Workshop on Advanced Materials for High Precision Detectors, pages 179-187.

[22] T.J.Adye et al.
The design and Operation of the Slow Controls for the DELPHI experiment at LEP
Nucl. Inst. and Meth. **A349** (1994), 160-182.

[23] S. Kersten, *Slow Control for the DELPHI Pixel Detector*, University of Wuppertal, May 9, 1997, available via WWW:
$http://www.uni-wuppertal.de/FB8/groups/Drees/detlab/vft\_slowctrl.html$

[24] J.M.Heuser, M. Caccia, L. Roos, *Online monitoring of the DELPHI VFT pixel detector*, DELPHI note 96–150 MVX 19, October 24, 1996

[25] V.Chorowicz, *The real-time monitoring in DELPHI*, Delphi note 95–30 DAS 163, March 6, 1995.

[26] M. Krammer, H. Pernegger, *Signal collection and position reconstruction of silicon strip detectors with 200 μm readout pitch*, HEPHY–PUB–648–96, Nucl. Inst. and Meth. **A397** (1997) 232–242
C. Troncon, *Measurement of spatial resolution and charge collection in double-sided double-metal silicon microstrip detectors* Nucl. Phys. Proc. Suppl. B 44 (1995), 287–291
P. Seller et al. *Noise in detectors and readout circuits*, RAL TR 96–001.

[27] V.Chabaud, A.Andreazza, P.Collins, H.Dijkstra, *Alignment of the DELPHI vertex detector*, DELPHI note 95–177 MVX 10, December 1995.

[28] A. Andreazza et al., ”*Results on the DELPHI microvertex alignment from a precise 3-D mapping*, Nucl. Instr. and Meth., **A312** (1992) 431.

S. Testa, Tesi di Laurea in Fisica, Università degli Studi di Milano, Milano, luglio 1993.
E. Bravin, Tesi di Laurea in Ingegneria, Politecnico di Milano, Milano, dicembre 1995.

[29] A.S. Moszczyński, *The Barycentric Effect in Semiconductor Position Sensitive Detectors*, REPORT No. 1749/PH, Institute of Nuclear Physics, Cracow.

[30] G.Borisov and C.Mariotti, *Performance of b-tagging in DELPHI at LEP2*, preprint CEN SACALY DAPNIA/SPP-97-06 and INFN-ISS 97/3, April 1997.

[31] P. Abreu et al., (DELPHI Collaboration), *Search for neutral and charged Higgs bosons in e^+e^- collisions at $\sqrt{s} = 161$GeV and 172GeV*, submitted to Zeit. Phys. C.

[32] M.A. Bizouard, private communication.